



Multi-response mathematical modelling, optimization and prediction of weld bead geometry in gas tungsten constricted arc welding (GTCAW) of Inconel 718 alloy sheets for aero-engine components

Tushar Sonar¹ · Visvalingam Balasubramanian¹ · Sudersanan Malarvizhi¹ · Thiruvengatam Venkateswaran² · Dhenuvakonda Sivakumar²

Received: 18 March 2020 / Accepted: 13 June 2020 / Published online: 1 July 2020

© Springer Nature Switzerland AG 2020

Abstract

The gas tungsten constricted arc welding (GTCAW) parameters namely Main Current, Delta Current, Delta Current Frequency and Welding Speed were optimized to obtain full penetration and optimum weld bead geometry using Response Surface Methodology (RSM) to join thin Inconel 718 alloy sheets (2 mm thick). Empirical relationships were formulated to predict the weld bead characteristics such as width of bead, depth of penetration, width of heat affected zone (HAZ) and area of fusion zone (FZ). The weld bead characteristics were predicted with good accuracy using developed empirical relationships. The direct and interaction effect of GTCAW parameters on weld bead geometry is discussed in this paper.

Keywords Gas tungsten constricted arc welding (GTCAW) · Inconel 718 alloy · Optimization · Mathematical modelling · Response surface methodology · Weld bead geometry

1 Introduction

Inconel 718 is a high-performance, precipitation hardened nickel-base superalloy widely used in aero-engine applications at elevated temperature up to 650 °C due to its excellent mechanical properties and weldability (Radhakrishna

and Rao 1994). It finds major applications in gas turbine blades, casings, rotors, discs etc. (Henderson et al. 2004). It exhibits excellent high temperature strength, exceptional creep and stress rupture properties, good resistance to oxidation and corrosion (Ram et al. 2005a, b). The solid solution strengthening is achieved by the addition of Cr, Co, W, Mo and V whereas the addition of Al, Ti and Nb provides precipitation hardening by the precipitation of γ' [$\text{Ni}_3(\text{Al}, \text{Ti})$] and γ'' [Ni_3Nb] phases (Pollock and Tin 2006). The γ'/γ'' microstructure can be maintained stable at higher ratios of (Al + Ti)/Nb and Al/Ti (Xie et al. 2007). The stable $\gamma''-\gamma'$ microstructure is important for its strength at elevated temperature (Liu et al. 2018).

Gas tungsten arc welding (GTAW) process is widely employed for joining Inconel 718 alloy sheets in manufacturing and service repair jobs of aero-engine components as it provides clean, precise and high-quality welds. Also, it is cost effective and shop friendly. However, the welding of Inconel 718 alloy is mainly constrained by the segregation of alloying elements and evolution of coarse thick film of laves phase in weld metal due to the high heat input in GTAW process (Radhakrishna et al. 1995). The laves phase evolution is detrimental to the weld tensile properties and joint performance (Ram et al. 2004; Sivaprasad et al. 2006). This alloy also shows extreme propensity for the hot cracking problems

✉ Tushar Sonar
tushar.sonar77@gmail.com

Visvalingam Balasubramanian
visvabalu@yahoo.com

Sudersanan Malarvizhi
jeejoo@rediffmail.com

Thiruvengatam Venkateswaran
tvenkateswaran@gmail.com

Dhenuvakonda Sivakumar
d_sivakumar@vssc.gov.in

¹ Centre for Materials Joining and Research (CEMAJOR), Department of Manufacturing Engineering, Annamalai University, Annamalai Nagar, Chidambaram 608 002, Tamilnadu State, India

² Heat Treatment and Welding Metallurgy Division (HWMD), Materials and Metallurgy Group (MMG), Vikram Sarabhai Space Centre (VSSC), ISRO, Thiruvananthapuram 695 022, Kerala State, India

such as liquation cracking in HAZ due to the evolution of low melting point eutectics at the grain boundaries (Hong et al. 2008). Moreover, the joining of metal sheets is more challenging to attain good weld bead without any defects, porosity and distortion. The high heat input in GTAW process is mainly associated with the low energy density due to the wider bell-shaped arc column.

To overcome this problem, gas tungsten constricted arc welding (GTCAW) process is employed to join thin Inconel 718 alloy sheets. It is an emerging variant of GTAW process, principally differentiated by magnetic arc constriction and high frequency pulsing of current up to 20 kHz (Leary et al. 2010a, b). It offers greater control over the welds which makes them preferable for critical aerospace applications. The magnetic arc constriction significantly minimizes the heat input and HAZ problems along with increased arc penetration during welding (Leary et al. 2010a, b). In GTCAW welding process, Delta Current is superimposed on Main Current to produce a magnetic field and constrict the arc. Delta Current (DC) pulses with Main Current at a very high frequency of up to 20 kHz in sawtooth shape waveform rather than square waveform as in Pulse Current GTAW. The arc constriction minimizes the heat input in welding by reducing the wastage of heat on outer flare and localized melting of metal at the joint. This allows for better heat management on welds whilst attaining full penetration. Figure 1 shows the comparison between the welding arc of GTCAW and GTAW process.

The input parameters have significant influence on the evolution of microstructure, weld bead profile and the mechanical properties of welded joints. Thus, the reliability and efficiency of welded components is highly contingent on the welding process parameters. This causes the need for developing techniques to search for optimized process parameters and

investigate its interaction effect on mechanical properties of welded joints. Since optimization of process parameters is costly and time-consuming, there is an approach to apply statistical methods such as design of experiments (DOE). Response surface methodology (RSM) is among the main strategies of DOE that can be applied to disclose unknown techniques through the use of an empirical mathematical model (Antony 2003; Montgomery 1997). It is a collection of mathematical and statistical approach used for formulation of mathematical model (Kiaee and Aghaie-Khafri 2014). By applying the technique of RSM, it is practicable to investigate the interaction effect of input parameters on joint properties and to optimize them to attain feasible results (Padmanaban and Balasubramanian 2011). Researchers have used the statistical approach of RSM to correlate the welding parameters to the mechanical properties of welded joints (Balasubramanian et al. 2008a, b; Razal Rose et al. 2012).

The investigations on welding of Inconel 718 alloy mainly pertains to the weldability studies with regard to gas tungsten arc welding (GTAW) (Sudarshan Rao et al. 2012; Cortés et al., 2017; Rodríguez et al., 2017), electron beam welding (EBW) (Reddy et al. 2008; Mei et al. 2016; Ram et al. 2005a, b) and laser beam welding (LBW) (Cao et al. 2009; Zhang et al. 2013; Ram et al. 2005a, b) processes. Furthermore, the information available on the recently emerged gas tungsten constricted arc (GTCAW) welding process in joining of Inconel 718 alloy sheets is limited. The smaller weld bead geometry results in lower laves phase content and reduced microfissuring tendency. So, the main purpose of this study is to optimize GTCAW welding parameters for joining Inconel 718 alloy sheets (2 mm thick) to attain optimum weld bead geometry and complete penetration.

2 Experimental methodology

2.1 Materials and specimen preparation

Rolled Inconel 718 alloy sheets of 2 mm thickness (solutionized at 980 °C) were used in the present study. The base material composition and mechanical properties are listed in Tables 1 and 2 separately. These sheets were cut to the required dimensions by abrasive cutting wheel. The edge surfaces to be welded were machined with cylindrical grinding machine. The surface oxide film was first removed by steel wire brushing and emery paper. The sheets were then cleaned chemically before welding by lint free cloth immersed in acetone solution to eliminate the surface contaminants. These sheets were welded in square butt joint design as illustrated

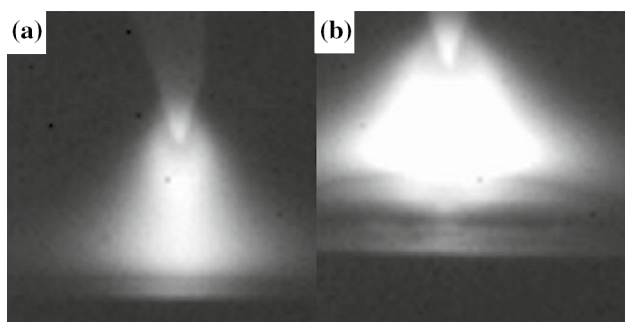


Fig. 1 a Constricted arc in GTCAW and (b) Wider arc in conventional GTAW process

Table 1 Base metal composition (% by weight)

Ni	Cr	Fe	Co	Mo	Nb	Ti	Al	C	Mn	Si	B	Cu	S
55.5	17.7	21.8	0.04	3.0	4.96	0.93	0.44	0.43	0.017	0.06	0.003	0.001	0.004

Table 2 Base metal mechanical properties

Tensile strength (MPa)	0.2% yield strength (MPa)	Elongation in 50 mm gauge length (%)	Notch tensile strength (MPa)	Notch strength ratio (NSR)	Micro-hardness (HV _{0.5})
870	580	38	805	0.92	292

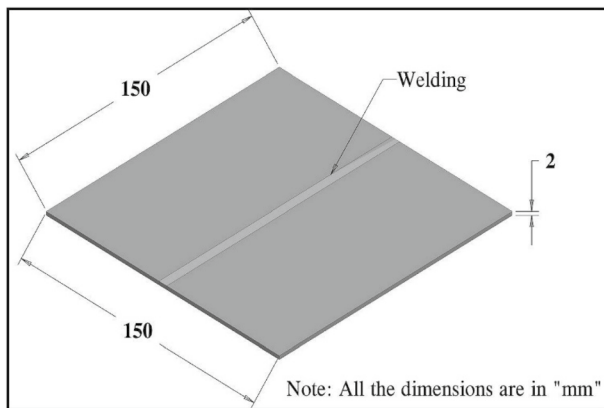


Fig. 2 Butt joint design used for welding sheets

in Fig. 2. The direction of welding was kept normal to the rolling direction.

2.2 Identification of welding process parameters

The set-up of GTCAW machine (Make: VBCie, UK; Model: InterPulse IE175i) is shown in Fig. 3. The GTCAW parameters namely Main Current, Delta Current, Delta Current Frequency and Welding Speed were identified which have significant influence on the tensile properties and microstructure of Inconel 718 alloy joints using one variable at a time approach in previous investigations (Sonar et al. 2019, 2020).

2.3 Development of design matrix and fabrication of welded joints

Inclusive trial runs were conducted on the base material implementing different combinations of GTCAW parameters to fix the feasible working limit for the design of experimental matrix. Bead appearance, full penetration, sound welds without porosity, undercuts, burn through related defects were set as the criteria for fixing the working range. Full factorial, Fractional factorial and Central Composite Design (CCD) matrix are typically practised for modelling the process responses. However, CCD pertains to the reduced number of experimental runs. So, the

Fig. 3 GTCA welding machine arrangement used to weld sheets

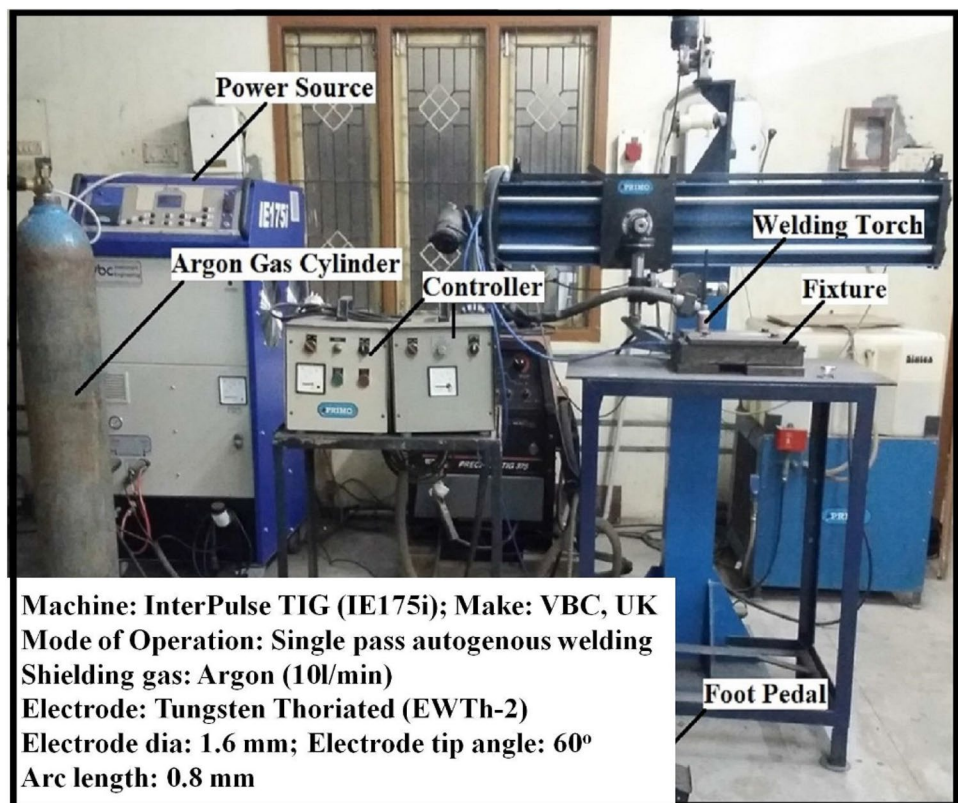










Table 3 Working limits of GTCA welding parameters

Sr. No	Parameters	Parameter Range	Macrostructure	Observation
1	Main Current	> 75 (A)		Deeper penetration and weld drop out
2	Main Current	< 55 (A)		Incomplete penetration
3	Delta Current	> 55 (A)		Deeper penetration and weld drop out
4	Delta Current	< 45 (A)		No penetration
5	Delta Current Frequency	20 (kHz)		Final limit and no defect
6	Delta Current Frequency	< 4 (kHz)		Bead appearance was similar to those of pulsed GTA welds
7.	Welding Speed	> 70 (mm/min)		Partial penetration
8.	Welding Speed	< 50 (mm/min)		Wider bead, Excess penetration and sheet burning

CCD matrix was selected in the present investigation for the optimization of GTCAW parameters. It comprises 30 sets of experimental runs ($2^k = 16$ factorial points, $2k = 8$ axial points and $n_c = 6$ centre points), 4 welding parameters and 5 levels ($\pm \alpha$, ± 1 and 0). Table 3 shows feasible working range of GTCA welding parameters in joining 2 mm thick Inconel 718 alloy sheets. The factors and levels used for the design of experiment are listed in Table 4. Table 5 represents the four factors—five levels central composite matrix drafted by Design-Expert 8.0 software for the

optimization experiment. The coded conditions +2 and -2 sign shows the upper and lower level of the factors separately. Autogenous butt welds were produced effectively with Gas Tungsten Constricted Arc (GTCA) welding machine as per the sequence of DOE. The welding was performed in delta straight arc mode in which Delta Current is pulsing with Main current in saw tooth shape wave form. The shielding was provided with pure Argon gas at a constant flow rate of 10 L/min. Thoriated Tungsten electrode (EWTh-2) of diameter 1.6 mm was used at an arc length of 0.8 mm and 60° electrode tip angle. Figure 4

Table 4 Feasible GTCA welding parameters and their levels

No	Parameter	Notations	Unit	-2	-1	0	+1	+2
1	Main Current (MC)	M	A	55	60	65	70	75
2	Delta Current (DC)	D	A	45	47.5	50	52.5	55
3	Delta Current Frequency (DCF)	F	kHz	4	8	12	16	20
4	Welding Speed (WS)	S	mm/min	50	55	60	65	70

Table 5 Design matrix and experimental results

Expt. No	<i>M</i>	<i>D</i>	<i>F</i>	<i>S</i>	<i>M</i>	<i>D</i>	<i>F</i>	<i>S</i>	WB (mm)	DP (mm)	HZ (mm)	FZ (mm ²)
1	-1	-1	-1	-1	60	47.5	8	55	4.81	2.17	0.39	8.5
2	1	-1	-1	-1	70	47.5	8	55	5.78	2.53	0.51	10.06
3	-1	1	-1	-1	60	52.5	8	55	5.25	2.35	0.51	8.63
4	1	1	-1	-1	70	52.5	8	55	6.1	2.55	0.56	10.44
5	-1	-1	1	-1	60	47.5	16	55	5.08	2.26	0.48	8.82
6	1	-1	1	-1	70	47.5	16	55	5.84	2.55	0.53	10.5
7	-1	1	1	-1	60	52.5	16	55	5.66	2.45	0.56	8.9
8	1	1	1	-1	70	52.5	16	55	6.32	2.61	0.58	10.77
9	-1	-1	-1	1	60	47.5	8	65	3.84	1.87	0.17	6.87
10	1	-1	-1	1	70	47.5	8	65	5.06	2.26	0.41	7.68
11	-1	1	-1	1	60	52.5	8	65	4.2	2.08	0.3	7.28
12	1	1	-1	1	70	52.5	8	65	5.26	2.34	0.46	8.27
13	-1	-1	1	1	60	47.5	16	65	4.1	2	0.25	7.2
14	1	-1	1	1	70	47.5	16	65	5.14	2.37	0.44	8.04
15	-1	1	1	1	60	52.5	16	65	4.62	2.21	0.34	7.59
16	1	1	1	1	70	52.5	16	65	5.48	2.46	0.48	8.62
17	-2	0	0	0	55	50	12	60	4.26	1.96	0.36	7.76
18	2	0	0	0	75	50	12	60	6.12	2.55	0.52	10.43
19	0	-2	0	0	65	45	12	60	4.77	2.21	0.42	7.85
20	0	2	0	0	65	55	12	60	5.58	2.46	0.5	8.6
21	0	0	-2	0	65	50	4	60	4.61	2.2	0.36	7.54
22	0	0	2	0	65	50	20	60	5.1	2.41	0.51	8.25
23	0	0	0	-2	65	50	12	50	6.23	2.62	0.61	11.23
24	0	0	0	2	65	50	12	70	4.43	2.16	0.25	7.46
25	0	0	0	0	65	50	12	60	4.52	2.26	0.43	7.64
26	0	0	0	0	65	50	12	60	4.53	2.26	0.44	7.65
27	0	0	0	0	65	50	12	60	4.54	2.26	0.45	7.64
28	0	0	0	0	65	50	12	60	4.55	2.26	0.47	7.66
29	0	0	0	0	65	50	12	60	4.51	2.28	0.42	7.66
30	0	0	0	0	65	50	12	60	4.5	2.26	0.41	7.66

WB Width of Bead, DP Depth of Penetration, FZ Area of Fusion Zone, HZ Width of Heat Affected Zone

shows Inconel 718 alloy sheets joined by GTCA welding process.

2.4 Macrostructure

The cross-sectional surface of the metallographic specimens was mirror finished using different grades of emery papers and diamond paste. The mirror polished surface was then etched with Kalling's reagent for revealing the macrostructure. The macrostructure of weld bead for different experimental runs was captured using a stereozoom microscope. The weld bead characteristics namely width of bead (WB), depth of penetration (DP), average width of HAZ (HZ) and area of fusion zone (FZ) were measured by ImageJ analysis software. Figure 5

shows the macrostructure of weld bead at different experimental runs.

3 Results and discussion

3.1 Formulation of mathematical model

The process parameters namely Main Current, Delta Current, Delta Current Frequency and Welding Speed were coded as M, D, F and S respectively. The response for the welded joints was recorded for width of bead (WB), depth of penetration (DP), average width of HAZ (HZ) and area of fusion zone (FZ).



Fig. 4 GTCA welded joints of Inconel 718 alloy

The response surface (Y) as a function of GTCAW parameters is illustrated as follows.

$$Y = f(M, D, F, S) \tag{1}$$

The regression model was subjected to multiple regression analysis corresponding to the response function of second order. The polynomial regression equation of second order used to illustrate the response surface ‘ Y ’ is given as:

$$Y = b_0 + \sum b_i x_i + \sum b_{ii} x_i^2 + \sum b_{ij} x_i x_j + e_r \tag{2}$$

The 4-factor polynomial regression equation of second order is illustrated as

$$Y = b_0 + b_1(M) + b_2(D) + b_3(F) + b_4(S) + b_{11}(M^2) + b_{22}(D^2) + b_{33}(F^2) + b_{44}(S^2) + b_{12}(MD) + b_{13}(MF) + b_{14}(MS) + b_{23}(DF) + B_{24}(DS) + B_{34}(FS) \tag{3}$$

where Y is the response, X_i and X_j are the coded independent variables, b_0 is the mean values of responses and b_i , b_{ii} and b_{ij} are the coefficients that depends on the linear, quadratic and interaction effect of GTCAW parameters respectively.

The values of the regression coefficients could be calculated by the following equations well reported in the literature.

$$b_0 = 0.142857(\sum aY) - 0.035714 \sum a \sum a (X_{ii}Y) \tag{4}$$

$$b_i = 0.041667(\sum aX_iY) \tag{5}$$

$$b_{ii} = 0.03125 \sum a(X_{ii}Y) + 0.00372 \sum a \sum a (X_{ii}Y) - 0.035714(\sum aY) \tag{6}$$

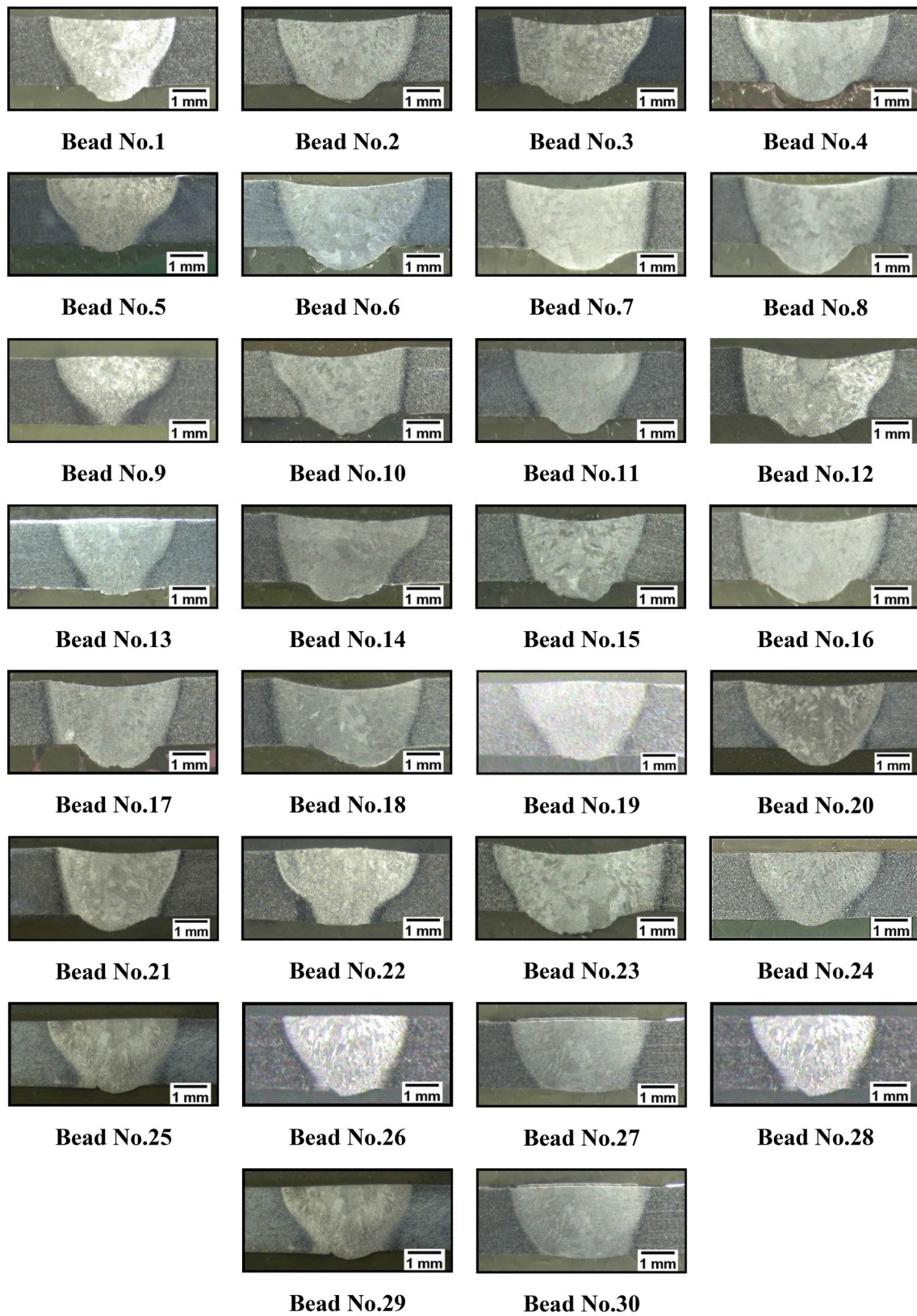


Fig. 5 Macrostructure of weld bead at different experimental runs

$$b_{ij} = 0.0625 \sum a(X_{ij}Y) \quad (7)$$

The Design-Expert 8.0 software was used to calculate the regression coefficients of the second order polynomial regression model at 95% confidence level. The initial mathematical models were formulated using the coefficients obtained from the above calculations. *T*-test and backward elimination method (available in software) was conducted to analyse the significance of the coefficients. The insignificant coefficients in addition to the corresponding responses were eliminated without compromising on the accuracy and finally mathematical model was developed using significant coefficients. The final formulated mathematical model with significant coefficient and input parameters is given below:

$$\begin{aligned} \text{WB, Width of Bead (mm)} = & +4.53 + 0.4642(\text{M}) + 0.2025(\text{D}) + 0.1217(\text{F}) - 0.4475(\text{S}) \\ & - 0.0350(\text{MD}) - 0.0487(\text{MF}) + 0.0588(\text{MS}) + 0.0375(\text{DF}) - 0.0250(\text{DS}) + 0.0013(\text{FS}) \\ & + 0.1698(\text{M}^2) + 0.1660(\text{D}^2) + 0.0860(\text{F}^2) + 0.2048(\text{S}^2) \end{aligned}$$

$$\begin{aligned} \text{DP, Depth of Penetration (mm)} = & +7.46375 + 0.145250(\text{M}) - 0.118667(\text{D}) - 0.033646(\text{F}) \\ & - 0.256833(\text{S}) - 0.002700(\text{MD}) - 0.000437(\text{MF}) + 0.000650(\text{MS}) + 0.000375(\text{DF}) \\ & + 0.0007(\text{DS}) + 0.000688(\text{FS}) - 0.000117(\text{M}^2) + 0.002733(\text{D}^2) + 0.000599(\text{F}^2) + 0.001233(\text{S}^2) \end{aligned}$$

$$\begin{aligned} \text{HZ, Width of HAZ (mm)} = & +0.4373 + 0.0537(\text{M}) + 0.0321(\text{D}) + 0.0271(\text{F}) - 0.0829(\text{S}) \\ & - 0.0144(\text{MD}) - 0.0106(\text{MF}) + 0.0306(\text{MS}) - 0.0056(\text{DF}) + 0.0006(\text{DS}) - 0.0006(\text{FS}) \end{aligned}$$

$$\begin{aligned} \text{FZ, Area of Fusion Zone (mm}^2\text{)} = & +7.65 + 0.6636(\text{M}) + 0.1804(\text{D}) + 0.1721(\text{F}) - 0.9421(\text{S}) \\ & + 0.0506(\text{MD}) + 0.0156(\text{MF}) - 0.2031(\text{MS}) - 0.0119(\text{DF}) + 0.0694(\text{DS}) - 0.0006(\text{FS}) \\ & + 0.3601(\text{M}^2) + 0.1426(\text{D}^2) + 0.0601(\text{F}^2) + 0.4226(\text{S}^2) \end{aligned}$$

where M = Main Current, D = Delta Current, F = Delta Current Frequency and S = Welding Speed.

3.2 Checking competency of the formulated Empirical Relationships

Analysis of Variance (ANOVA) and regression analysis was used to assess the competency of formulated model. Tables 6, 7, 8, 9 show the results of ANOVA for the width of bead, depth of penetration, width of HAZ and area of FZ, respectively. The *F* value and the associated *p*-values of the respective models were used to confirm the competency of the formulated mathematical relationships. Furthermore, the controlling factors that have significant and subsidiary influence on the responses could be investigated using *F* values. The model is supposed to be competent if the standard *F* ratio (from table) is greater than the calculated *F* ratio of the

formulated model at a given confidence level. It is evident that the formulated relationship is competent at 95% confidence level. The calculated *F* values of 2760.09, 733.42, 57.06 and 10,404.03 for the weld bead responses (width of bead, depth of penetration, width of HAZ and area of FZ) indicate that the relationship is significant. There are only 0.01% chances of occurring this high “model *F* value” due to noise. The “prob > *F*” values are less than 0.05. It indicates the significant events of the relationship terms. Values greater than 0.1 indicate that the relationship terms are insignificant. The *F* value is higher for Main Current in ANOVA tables of bead width (WB) and depth of penetration (DP). It is attributed to the widening of the arc and increase in arc force associated with increased levels of Main

Current. Increase in Main Current results in increased number of electrons striking the workpiece. This gives rise to the magnitude of arc force acting on the weld pool which tends to increase the depth of penetration. Also, with increase in Main Current the diameter of the arc column becomes wider which reduces the arc constriction effect and leads to increase in bead width. However, in case of fusion zone (FZ) and heat affected zone (HZ), Welding Speed showed larger *F* value. It is attributed to the significant reduction in heat input and increase in cooling rate associated with incremental levels of Welding Speed. Increase in Welding Speed reduces the heat input and melting of metal at the joint. This leads to significant reduction in area of FZ and width of HAZ at increased level of Welding Speed. It reduces the peak temperature immediately in the area surrounding the weld pool and enhances the cooling rate. Hence the Welding

Table 6 ANOVA test results for Width of Bead (WB)

Source	Sum of squares	df	Mean square	F value	P value	
Model	13.59	14	0.9706	2760.09	<0.0001	Significant
M-MC	5.17	1	5.17	14,703.74	<0.0001	
D-DC	0.9842	1	0.9842	2798.53	<0.0001	
F-DCF	0.3553	1	0.3553	1010.24	<0.0001	
S-WS	4.81	1	4.81	13,666.78	<0.0001	
MD	0.0196	1	0.0196	55.73	<0.0001	
MF	0.0380	1	0.0380	108.13	<0.0001	
MS	0.0552	1	0.0552	157.04	<0.0001	
DF	0.0225	1	0.0225	63.98	<0.0001	
DS	0.0100	1	0.0100	28.44	<0.0001	
FS	0.0000	1	0.0000	0.0711	0.7934	
M^2	0.7907	1	0.7907	2248.56	<0.0001	
D^2	0.7562	1	0.7562	2150.34	<0.0001	
F^2	0.2031	1	0.2031	577.42	<0.0001	
S^2	1.15	1	1.15	3271.12	<0.0001	
Residual	0.0053	15	0.0004			
Lack of fit	0.0035	10	0.0004	1.01	0.5314	Not significant
Pure error	0.0018	5	0.0004			
Cor total	13.59	29				
Fit statistics	Std. Dev	0.0188	R^2	0.9996		
	Mean	5.03	Adjusted R^2	0.9992		
	C.V. %	0.3731	Predicted R^2	0.9983		
			Adeq precision	186.3972		

Table 7 ANOVA test results for Depth of Penetration (DP)

Source	Sum of squares	df	Mean square	F value	p value	
Model	1.04	14	0.0746	733.42	<0.0001	Significant
M-MC	0.4988	1	0.4988	4906.39	<0.0001	
D-DC	0.0988	1	0.0988	971.97	<0.0001	
F-DCF	0.0580	1	0.0580	570.66	<0.0001	
S-WS	0.3267	1	0.3267	3213.11	<0.0001	
MD	0.0182	1	0.0182	179.26	<0.0001	
MF	0.0012	1	0.0012	12.05	0.0034	
MS	0.0042	1	0.0042	41.56	<0.0001	
DF	0.0002	1	0.0002	2.21	0.1576	
DS	0.0012	1	0.0012	12.05	0.0034	
FS	0.0030	1	0.0030	29.75	<0.0001	
M^2	0.0002	1	0.0002	2.30	0.1506	
D^2	0.0080	1	0.0080	78.74	<0.0001	
F^2	0.0025	1	0.0025	24.78	0.0002	
S^2	0.0261	1	0.0261	256.49	<0.0001	
Residual	0.0015	15	0.0001			
Lack of fit	0.0012	10	0.0001	1.79	0.2707	Not significant
Pure error	0.0003	5	0.0001			
Cor total	1.05	29				
Fit statistics	Std. Dev	0.0101	R^2	0.9985		
	Mean	2.31	Adjusted R^2	0.9972		
	C.V. %	0.4371	Predicted R^2	0.9930		
			Adeq precision	105.7190		

Table 8 ANOVA test results for Width of HAZ (HZ)

Source	Sum of squares	<i>df</i>	Mean square	<i>F</i> value	<i>p</i> value	
Model	0.2973	10	0.0297	57.06	<0.0001	Significant
M-MC	0.0693	1	0.0693	133.08	<0.0001	
D-DC	0.0247	1	0.0247	47.42	<0.0001	
F-DCF	0.0176	1	0.0176	33.79	<0.0001	
S-WS	0.1650	1	0.1650	316.70	<0.0001	
MD	0.0033	1	0.0033	6.35	0.0209	
MF	0.0018	1	0.0018	3.47	0.0782	
MS	0.0150	1	0.0150	28.80	<0.0001	
DF	0.0005	1	0.0005	0.9717	0.3367	
DS	6.250E-06	1	6.250E-06	0.0120	0.9139	
FS	6.250E-06	1	6.250E-06	0.0120	0.9139	
Residual	0.0099	19	0.0005			
Lack of fit	0.0076	14	0.0005	1.16	0.4709	Not significant
Pure error	0.0023	5	0.0005			
Cor total	0.3072	29				
	Std. Dev	0.0228	<i>R</i> ²	0.9678		
Fit statistics	Mean	0.4373	Adjusted <i>R</i> ²	0.9508		
	C.V. %	5.22	Predicted <i>R</i> ²	0.9217		
			Adeq precision	30.5982		

Table 9 ANOVA test results for Area of Fusion Zone (FZ)

Source	Sum of squares	<i>df</i>	Mean square	<i>F</i> value	<i>p</i> value	
Model	41.67	14	2.98	10,404.03	<0.0001	Significant
M-MC	10.57	1	10.57	36,956.05	<0.0001	
D-DC	0.7812	1	0.7812	2730.42	<0.0001	
F-DCF	0.7107	1	0.7107	2484.01	<0.0001	
S-WS	21.30	1	21.30	74,448.36	<0.0001	
MD	0.0410	1	0.0410	143.32	<0.0001	
MF	0.0039	1	0.0039	13.65	0.0022	
MS	0.6602	1	0.6602	2307.34	<0.0001	
DF	0.0023	1	0.0023	7.89	0.0132	
DS	0.0770	1	0.0770	269.15	<0.0001	
FS	6.250E-06	1	6.250E-06	0.0218	0.8845	
<i>M</i> ²	3.56	1	3.56	12,431.54	<0.0001	
<i>D</i> ²	0.5578	1	0.5578	1949.54	<0.0001	
<i>F</i> ²	0.0991	1	0.0991	346.32	<0.0001	
<i>S</i> ²	4.90	1	4.90	17,121.27	<0.0001	
Residual	0.0043	15	0.0003			
Lack of fit	0.0038	10	0.0004	3.94	0.0717	Not significant
Pure error	0.0005	5	0.0001			
Cor total	41.68	29				
	Std. Dev	0.0169	<i>R</i> ²	0.9999		
Fit statistics	Mean	8.44	Adjusted <i>R</i> ²	0.9998		
	C.V. %	0.2004	Predicted <i>R</i> ²	0.9995		
			Adeq precision	364.4262		

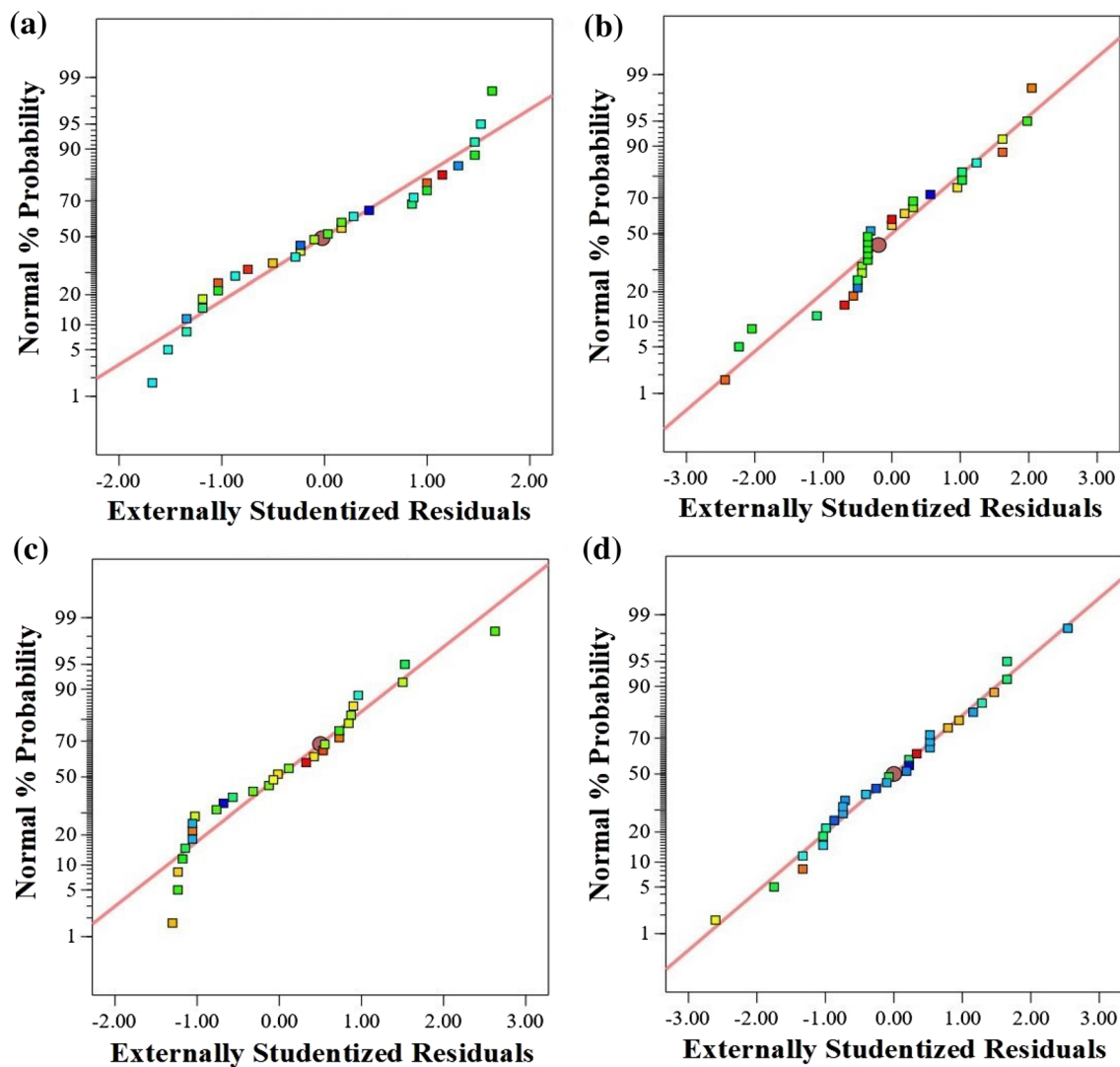


Fig. 6 Normal probability plot of residuals for weld bead responses: (a) width of bead; (b) depth of penetration; (c) width of HAZ; (d) area of fusion zone

Speed exhibits significant influence on area of fusion zone and width of HAZ.

The lack of fit is insignificant for all the responses as compared to the pure error. It is indicated by the respective “lack of Fit-value” of 1.01, 1.79, 1.16, 3.94. The chances of occurring higher values of “lack of fit” for the respective models are 53.14%, 27.07%, 47.09% and 7.17% respectively. The agreement of the experimental and predicted values was confirmed by the “coefficient of determination (r^2)”. The “Predicted R -Square” is in good agreement with the “Adjusted R -Square” values for all the formulated models. The signal to noise ratio is defined by the term “Adeq. Precision” which should be greater than 4 for desirability. The value of Adeq. precision differentiates the range of values predicted at the design points with the mean error of prediction. Simultaneously, the lower value of the coefficient of

variation (C.V) specifies the better precision and reliability of the experimental matrix. The Adeq. Precision ratio of 186.397, 105.719, 30.598, and 364.426 for the respective responses indicate competency of the model. The respective models for weld bead parameters can be used to navigate the design space. Figure 6 shows the normal probability plot of the residuals for weld bead responses. The residuals dropped on a straight line implies the normal distribution of errors. The considerations explained above confirms the competency of the formulated mathematical models and make it feasible for practical applications.

3.3 Validation of formulated mathematical model

The formulated mathematical models can be efficiently exploited to predict the weld bead responses by substituting

Table 10 Comparison of actual experimental value with RSM predicted value

Run order	Width of bead			Depth of penetration			Width of HAZ			Area of fusion zone		
	Actual value	Predicted value	% Error	Actual value	Predicted value	% Error	Actual value	Predicted value	% Error	Actual value	Predicted value	% Error
1	6.10	6.09	0.16	2.55	2.55	-0.39	0.56	0.55	1.81	10.44	10.43	0.10
2	5.58	5.59	-0.18	2.46	2.46	0.81	0.50	0.48	2.04	8.60	8.58	0.23
3	4.81	4.80	0.21	2.17	2.18	0.46	0.39	0.40	-2.50	8.50	8.48	0.24
4	5.84	5.85	0.17	2.55	2.56	0.39	0.53	0.55	-3.63	10.50	10.48	0.19
5	5.14	5.12	0.39	2.37	2.37	0.84	0.44	0.43	-2.32	8.04	8.05	-0.12

the values of input parameter in coded form. To validate the accuracy of formulated models, conformity test was conducted. The actual and predicted values of weld bead responses under different conditions of GTCAW parameters were compared from the design matrix and the % of error was also estimated illustrating the deviation of actual values with regard to the predicted values as shown in Table 10. It is observed that the average error for all models is less than 1% except for width of HAZ which was observed to be 2.08%. The actual experimental values are in close proximity with the values predicted by the formulated relationship as shown in Fig. 7. Perturbation plot comparing the influence of all the factors at a certain location in design space is shown in Fig. 8. It follows the strategy of one variable at a time of DOE in which the response is plotted by varying one parameter over its range while other parameters kept constant. By general settings, Design-Expert software fixes the reference point of all factors at the mid-point (coded 0). A steep slope or curvature associated with Welding Speed, Main Current and Delta Current in a plot illustrate the sensitivity of weld bead response at its respective levels. However, comparatively flat line associated with Delta Current Frequency represents the insensitivity to variation in that specific factor. The perturbation plot shows high sensitivity of weld bead responses to Welding Speed.

3.4 Optimization

The optimization module looks for a factor level combination that meet the criteria put on each of the responses and factors concurrently. The welding process is a multi-objective problem with an aim to attain full penetration, minimum bead width, HAZ width and fusion zone area for good quality weld and maximum welding speed for higher productivity. The formulated mathematical models were used for the optimization of GTCAW parameters to attain optimum weld bead geometry. Bead area is the key parameter of the weld bead, influenced by the other parameters such as depth of penetration, width of bead, and aspect ratio of weld bead. Good control over the weld bead region contributes to minimal heat input, better control over other bead configuration and also optimal use of the welding power source.

3.4.1 Numerical optimization

Numerical optimization implements the formulated mathematical models to look for the factor space for the best compromise on optimum solution to achieve multiple objectives (Rajkumar and Balasubramanian 2011). The optimization criterion is to attain full penetration and minimize the width of weld bead, HAZ and area of fusion zone. That is achieving the full penetration at comparatively lower power and increased welding speed in addition to sound, good quality

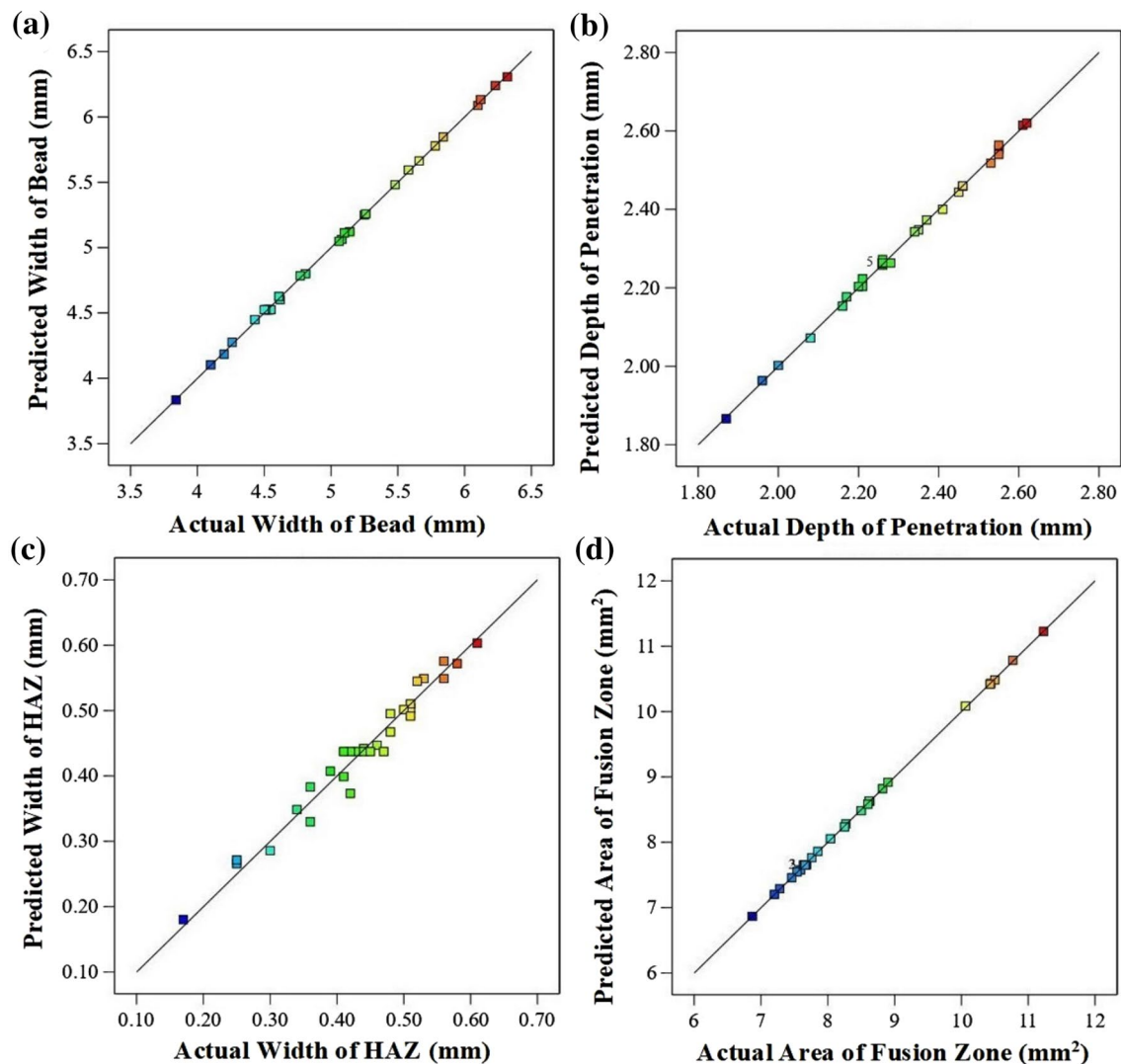


Fig. 7 Correlation plot for actual response values vs predicted response values

defect free weld joints. The objective, lower and upper limits as well as the importance for each response and factor in the optimization criteria is listed in Table 11.

Table 12 shows the list of GTCA welding parameters based on optimization criteria as determined by Design-Expert 8.0 software. The optimal welding conditions were preferred depending on the desirability function satisfying the criteria of optimization. The desirability ranges from 0.85 to 0.88 for any given response. The optimal welding parameters attaining maximum desirability function of 0.88 is selected. As Main Current is increased, DC and DCF need to be reduced at constant level of Welding Speed (70 mm/min) to meet the optimization criteria. Figure 9 shows the contour plot for numerical optimization results of weld bead responses. It represents the weld bead prediction satisfying the optimization criteria at the

corresponding optimal conditions. The predicted bead width of 4.28 mm, full penetration of 2.1 mm, HAZ width of 0.23 mm and FZ area of 7.43 mm² is achieved at Main Current of 63.12 A, DC of 49.67 A, DCF of 13.23 A and Welding Speed of 70 mm/min. Table 13 shows the optimum GTCA welding parameters obtained from the experimental design matrix and predicted by RSM. It shows that the experimental and predicted optimal welding conditions are in close proximity with each other. Also, the responses recorded under experimental and predicted conditions are in close agreement with each other.

3.4.2 Graphical optimization

Graphical optimization applies the formulated mathematical models to illustrate the factor space where it can find the

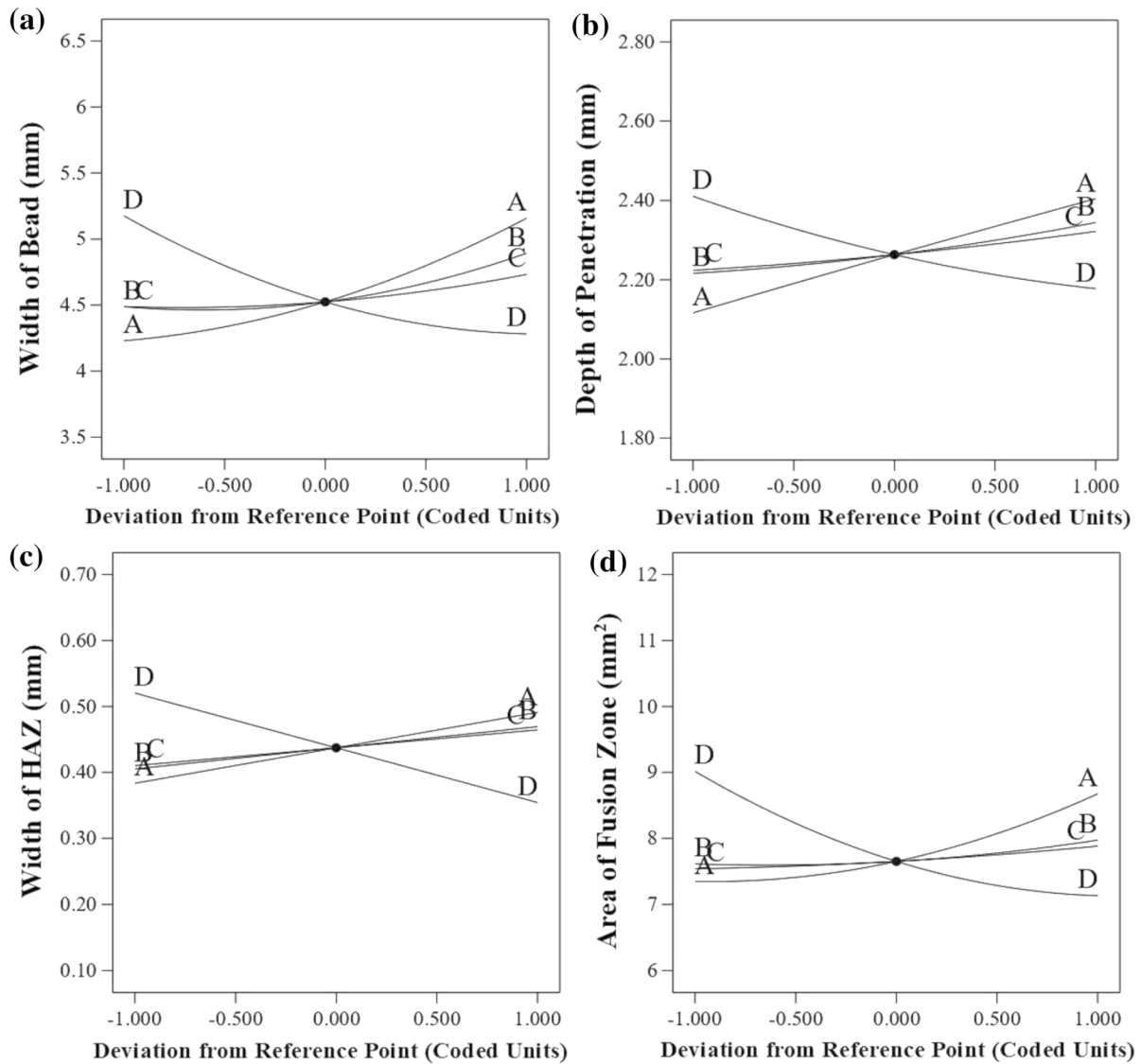


Fig. 8 Perturbation plot for weld bead responses: **(a)** width of bead; **(b)** depth of penetration; **(c)** width of HAZ; **(d)** area of fusion zone

Table 11 Criteria for numerical optimization

Name	Objective	Lower limit	Upper limit	Importance
Main Current (M)	In range	55	75	–
Delta Current (D)	In range	45	55	–
Delta Current frequency (F)	In range	4	20	–
Welding Speed (S)	Maximize	50	70	3
Width of Bead (WB)	Minimize	3.84	6.32	3
Depth of Penetration (DP)	In range	2.1	2.3	5
Width of HAZ (HZ)	Minimize	0.17	0.61	4
Area of Fusion Zone (FZ)	Minimize	6.87	11.23	5

reasonable response performance (Benyounis et al. 2005). The lower and upper limit were selected as per results of the numerical optimization. The performance criteria already

proposed in the numerical optimization, was set in the graphical optimization. The optimum area is shown by yellow

Table 12 Optimal welding solutions based on weld bead optimization criteria

Number	<i>M</i>	<i>D</i>	<i>F</i>	<i>S</i>	WB	DP	HZ	FZ	Desirability	Decision
1	63.126	49.673	13.231	70.000	4.287	2.100	0.233	7.432	0.881	Selected
2	63.151	49.673	13.186	70.000	4.287	2.100	0.233	7.430	0.881	
3	63.148	49.685	13.173	70.000	4.286	2.100	0.233	7.430	0.881	
4	63.130	49.686	13.200	70.000	4.286	2.100	0.233	7.432	0.881	
5	63.156	49.689	13.152	70.000	4.286	2.100	0.233	7.430	0.881	
6	62.947	47.379	16.624	69.999	4.483	2.100	0.225	7.541	0.860	
7	63.696	51.356	9.045	70.000	4.376	2.107	0.243	7.537	0.859	
8	64.823	46.778	13.647	69.999	4.553	2.100	0.238	7.364	0.859	
9	63.332	51.704	8.450	70.000	4.384	2.100	0.236	7.592	0.858	
10	65.974	48.689	8.751	70.000	4.518	2.100	0.256	7.282	0.856	

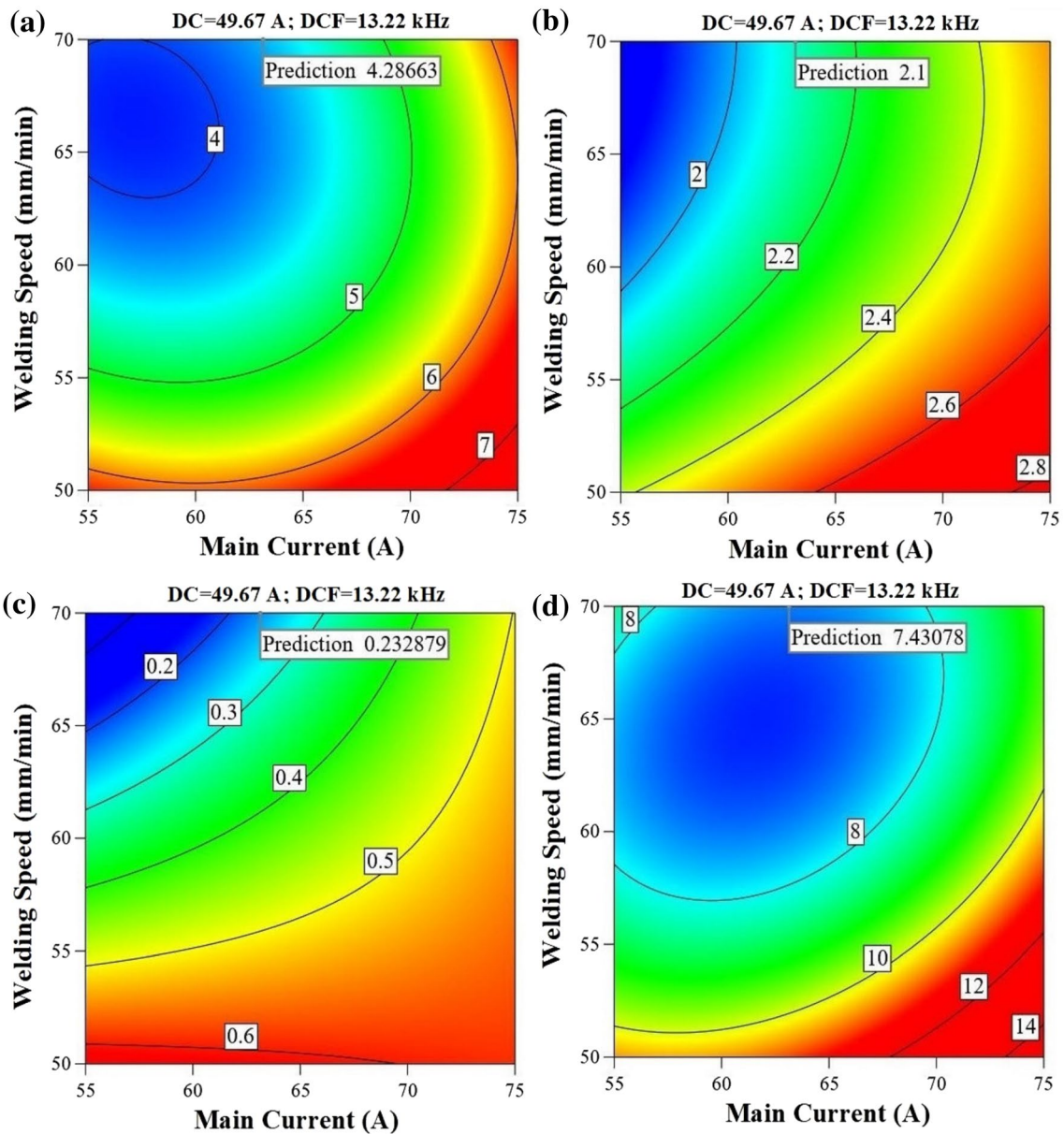
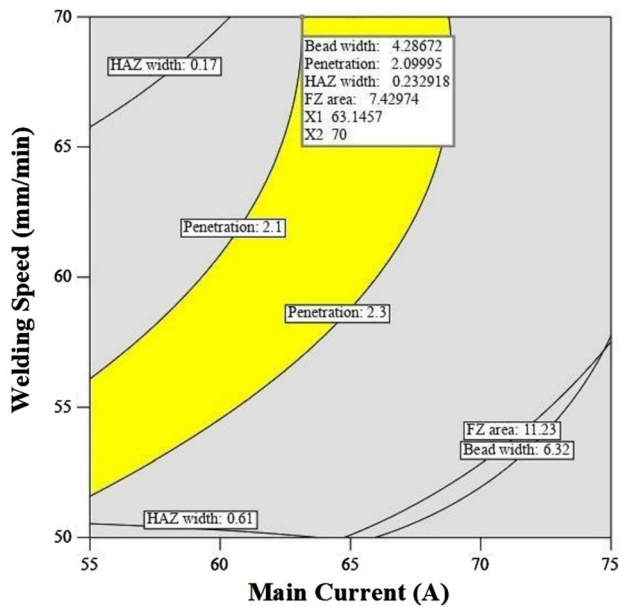


Fig. 9 Contour plots for numerical optimization results of weld bead responses: (a) width of bead; (b) depth of penetration; (c) width of HAZ; (d) area of fusion zone

Table 13 Optimized GTCA welding parameters

Condition	<i>M</i>	<i>D</i>	<i>F</i>	<i>S</i>	WB	DP	HZ	FZ
Experimental	65	50	12	70	4.43	2.16	0.25	7.46
Predicted by RSM	63.151	49.673	13.186	70.000	4.287	2.100	0.233	7.430

**Fig. 10** Overlay plot showing the optimized region graphically

coloured area in the Fig. 10. The grey coloured area shows the region that does not satisfy the optimality criteria.

3.5 Analysis of response surface graphs

3.5.1 Direct and interaction effect of GTCA welding parameters on width of bead

Figure 11a–d shows the direct effect of GTCAW parameters on the width of bead. It shows increase in bead width at increased levels of MC. As DC increases from 45 to 50 A bead width decreases. Further increase results in increase in bead width. Increase in DCF shows increase in bead width. However, increase in WS shows decrease in bead width due to the reduced heat input.

Figure 12a–f represents the three-dimensional response surface graph for width of bead, obtained from the regression model separately. The optimum value of response is represented by the descent area of the response surface. It shows that the weld bead is minimum at MC of 60 A, DC of 47.5 A, DCF of 8 kHz and WS of 65 mm/min. It also shows the interaction effect between two process parameters while assuming the remaining two parameters at constant level. Figure 12a shows the response surface plot for MC and DC assuming

DCF of 12 kHz and WS of 60 mm/min. The interaction effect between MC and DC indicates an increase in width of bead at their incremental levels. It is attributed to the increase in heat input and arc diameter with increase in MC and DC, resulting in more intense plasma jet and more melting of metal at the joint. This effect is more severe above MC of 65 A and DC of 50 A. The width of bead is observed to be much larger at higher levels of MC (75 A) and DC (55 A). Figure 12b shows the response surface plot for MC and DCF assuming the DC of 50 A and WS of 60 mm/min. It shows rise in width of bead at incremental levels of MC and DCF. It is attributed to the increase in heat input and arc diameter with increase in MC and stacking of heat input in weld thermal cycle at increased levels of DCF. This effect is remarkable above MC of 65 A and DCF of 12 kHz. The width of bead is much wider at higher level of MC (75 A) and DCF (20 kHz). Figure 12c represent the response surface plot for MC and WS assuming the DC of 50 A and DCF of 12 kHz. It implies that increase in MC and WS shows increase in bead width. The decrease in heat input by WS is counteracted by MC at incremental levels. The increase in width of bead becomes more severe above MC of 65 A and below WS of 60 mm/min. It shows wider bead width at higher level of MC (75A) and lower level of WS (50 mm/min).

Figure 12d represents the response surface plot for DC and DCF assuming MC of 65 A and WS of 60 mm/min. It shows the interaction effect between DC and DCF which is comparatively less significant as compared to the interaction effect of other parameters. Increase in DC and DCF shows slight increase in width of bead. There are no significant changes in width of bead up to DC of 50 A and DCF of 12 kHz. It represents wider width of bead at higher level of DC (55 A) and DCF (20 kHz). Figure 12e depicts the response surface plot for DC and WS assuming the MC of 65 A and DCF of 12 kHz. It indicates that an increase in DC and WS results in decrease in width of bead. This effect is pronounced above DC of 50 A and WS of 60 mm/min. The constricted arc maintains its stiffness and arc constriction at incremental levels of DC along with an increase in WS. The width of bead is wider at DC of 55 A and WS of 50 mm/min. Figure 12f depicts the response surface graph for DCF and WS assuming the MC of 65 A and DC of 50 A. It shows that interaction effect between DCF and WS is not significant. However, the width of bead is observed to be wider at WS of 50 mm/min and DCF of 20 kHz.

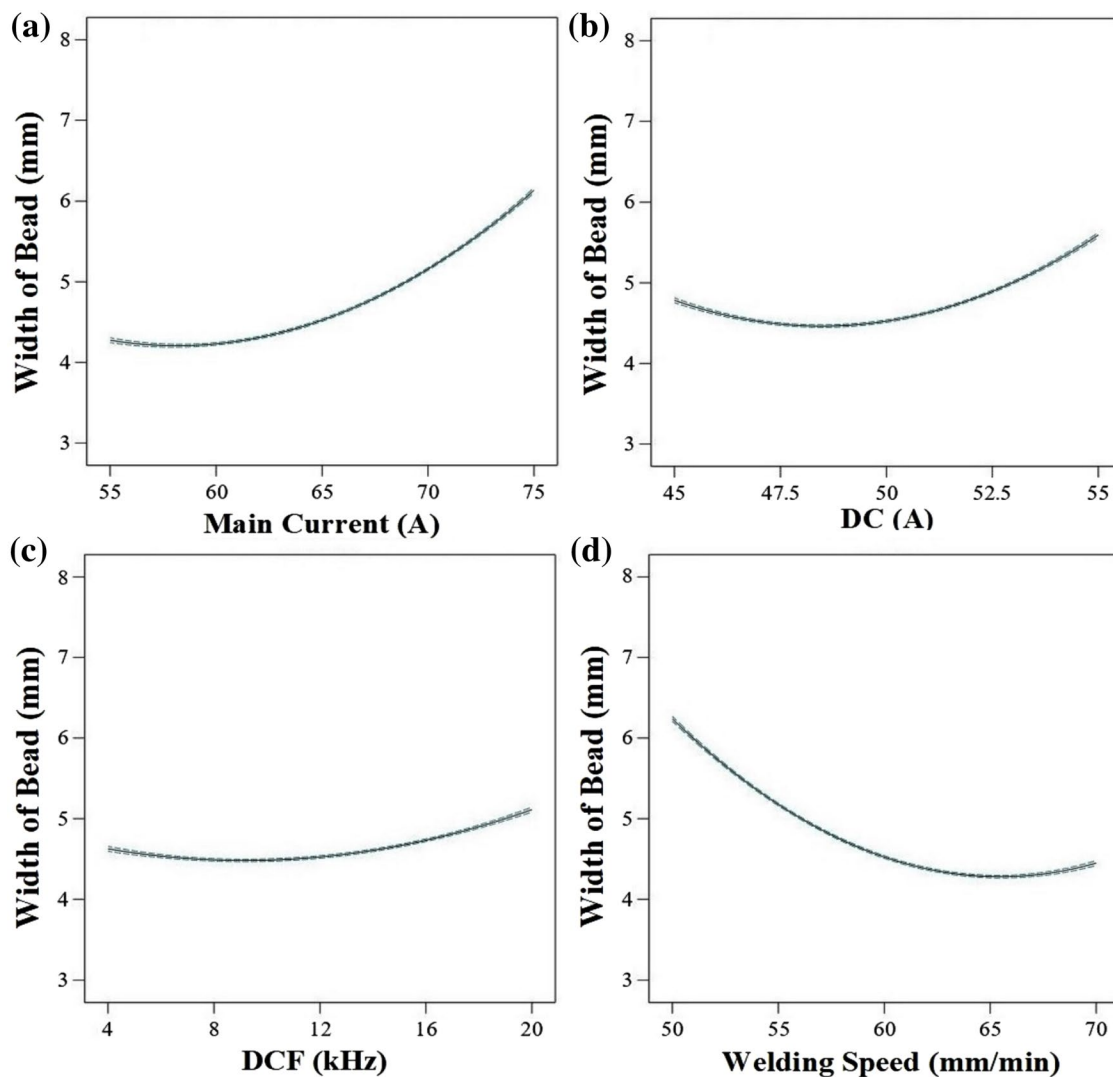


Fig. 11 Direct effect of GTCA welding parameters on width of bead

3.5.2 Direct and interaction effect of GTCA welding parameters on depth of penetration

Figure 13a–d shows the direct effect of GTCAW parameters on the depth of penetration. It shows that increase in MC leads to increase in penetration. It shows the straight-line proportional relationship of MC with penetration. The increase in DC shows slight increase in penetration up to 50 A. Further increase results in notable increase in penetration. DCF shows increase in penetration above 12 kHz. WS shows curved inverse relationship with penetration.

Figure 14a–f represents the three-dimensional response surface graph for the depth of penetration. The optimum value of response is to maximize the depth of penetration in the range of 2.1–2.3 mm. It shows that the depth of penetration is optimum at MC of 65 A, DC of 50 A, DCF of 12 kHz and WS of 60 mm/min. Figure 14a shows

the response surface plot for MC and DC assuming DCF of 12 kHz and WS of 60 mm/min. It shows that increase in MC and DC results in increased depth of penetration. The depth of penetration is more above MC of 65 A and DC of 50 A. It is attributed to the increased arc force with increase in MC and arc constriction at incremental levels of DC. The combined effect of MC and DC also leads to increased heat input at incremental levels contributing to the increased depth of penetration. It shows excess penetration at MC of 75 A and DC of 55 A. Figure 14b shows the response surface graph for MC and DCF assuming the DC of 50 A and WS of 60 mm/min. Increase in MC and DCF leads to the rise in depth of penetration. This effect is more severe above MC of 65 A and DCF of 12 kHz. It is attributed to the increase in heat input associated with incremental levels of MC and stacking of heat input in weld thermal cycles. It shows excess penetration at MC of 75 A and DCF of 20 kHz.

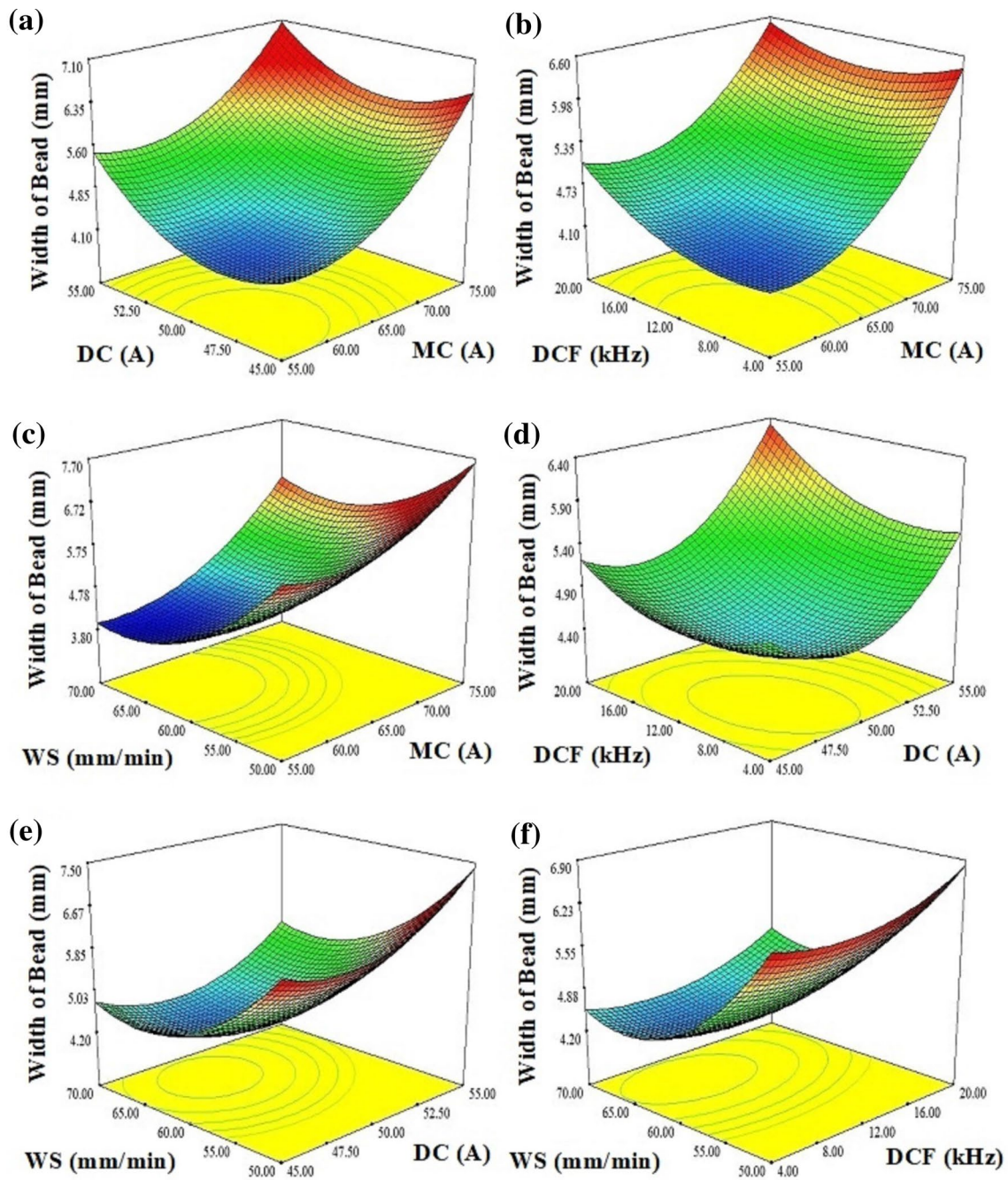


Fig. 12 3D Response Surface graphs for width of bead

Figure 14c represents the response surface graph for MC and WS assuming the DC of 50 A and DCF of 12 kHz. It indicates that increase in MC and WS leads to the increased depth of penetration. This effect is pronounced above MC of 65 A and below WS of 60 mm/min. However, the interaction effect between MC and WS is comparatively less significant than the individual direct effect of MC and WS. The depth of penetration is much deeper at higher level of MC (75 A) and lower level of WS (50 mm/min). Figure 14d represents

the response surface graph for DC and DCF assuming the MC of 65 A and WS of 60 mm/min. It represents that there is an insignificant interaction effect between DC and DCF on the depth of penetration. Figure 14e depicts the response surface graph for DC and WS assuming the MC of 65 A and DCF of 12 kHz. It shows that increase in DC and WS leads to increase in the depth of penetration. It is attributed to the fact that increase in DC at incremental levels of WS provides arc constriction stability and stiffness. Thus, the depth of

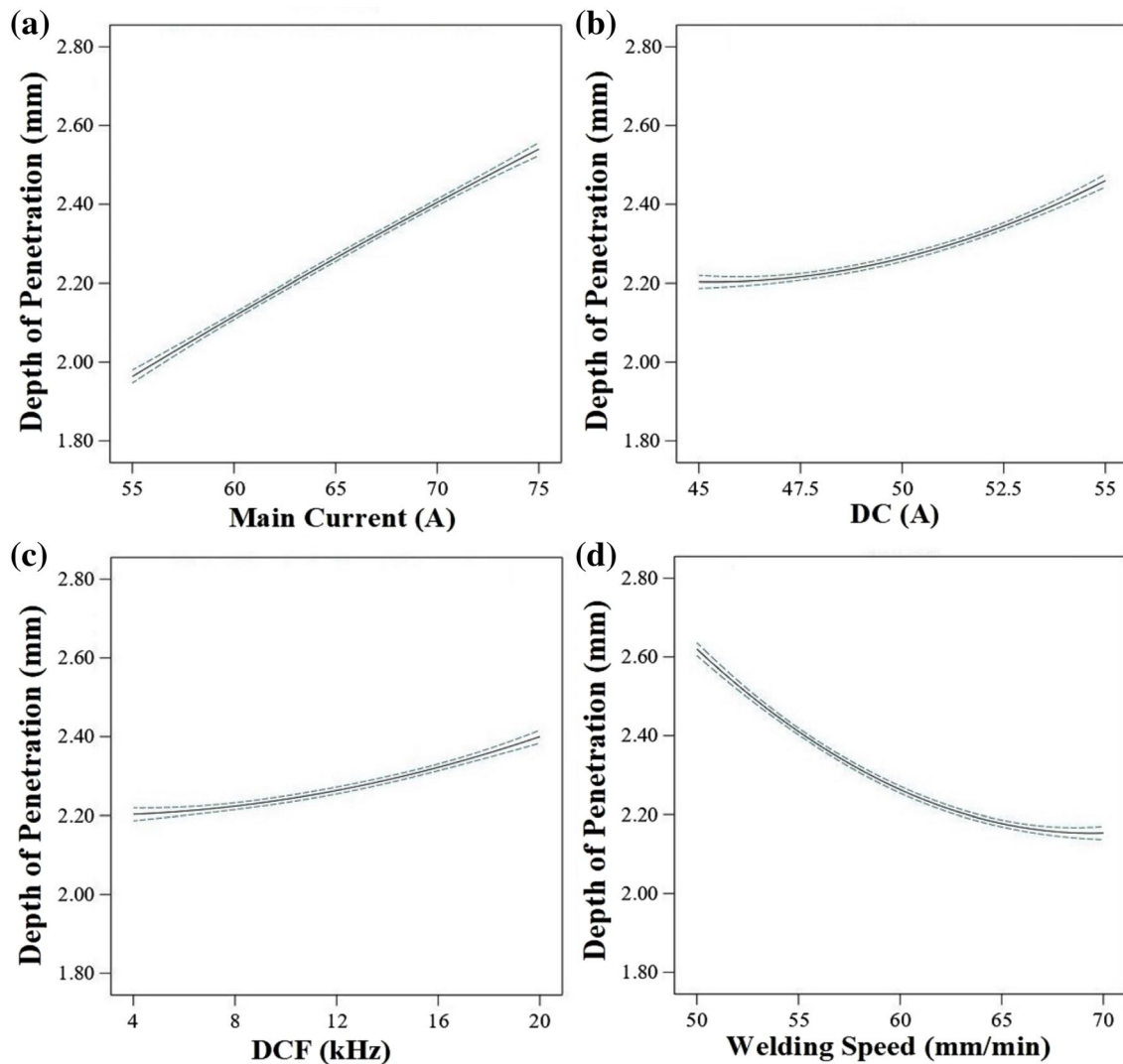


Fig. 13 Direct effect of GTCA welding parameters on depth of penetration

penetration increases significantly above DC of 50 A and below WS of 60 mm/min due to the more localized melting of metal at the joint. The depth of penetration is deeper at higher level of DC (55 A) and lower level of WS (50 mm/min). Figure 14f depicts the response surface graph for DCF and WS assuming the MC of 65 A and DC of 50 A. It indicates the interaction effect between DCF and WS. It shows slight increase in depth of penetration at increased levels of DCF and WS. However, their interaction effect is comparatively less significant than the individual direct effect of DCF and WS. The slight increase in depth of penetration is due to the reason that increase in WS is associated with reduction in heat input and it lowers the effect of piling of heat input observed in increased levels of DCF. The depth of penetration is more at higher level of DCF (20 kHz) and lower level of WS (50 mm/min).

3.5.3 Direct and interaction effect of GTCA welding parameters on width of HAZ

Figure 15a–d shows the direct effect of GTCAW parameters on width of HAZ. MC, DC, and DCF show straight-line proportional relationship with the width of HAZ. It is attributed to the increase in heat input associated with respective incremental levels of process parameters. WS shows inverse straight-line relationship with the width of HAZ. MC and WS shows significant effect on the width of HAZ followed by DC and DCF.

Figure 16a–f represents the three-dimensional response surface graph for the width of HAZ, obtained from the regression model separately. The optimum value of response is represented by the descent area of the response surface. It shows that the width of HAZ is minimum at MC of 60

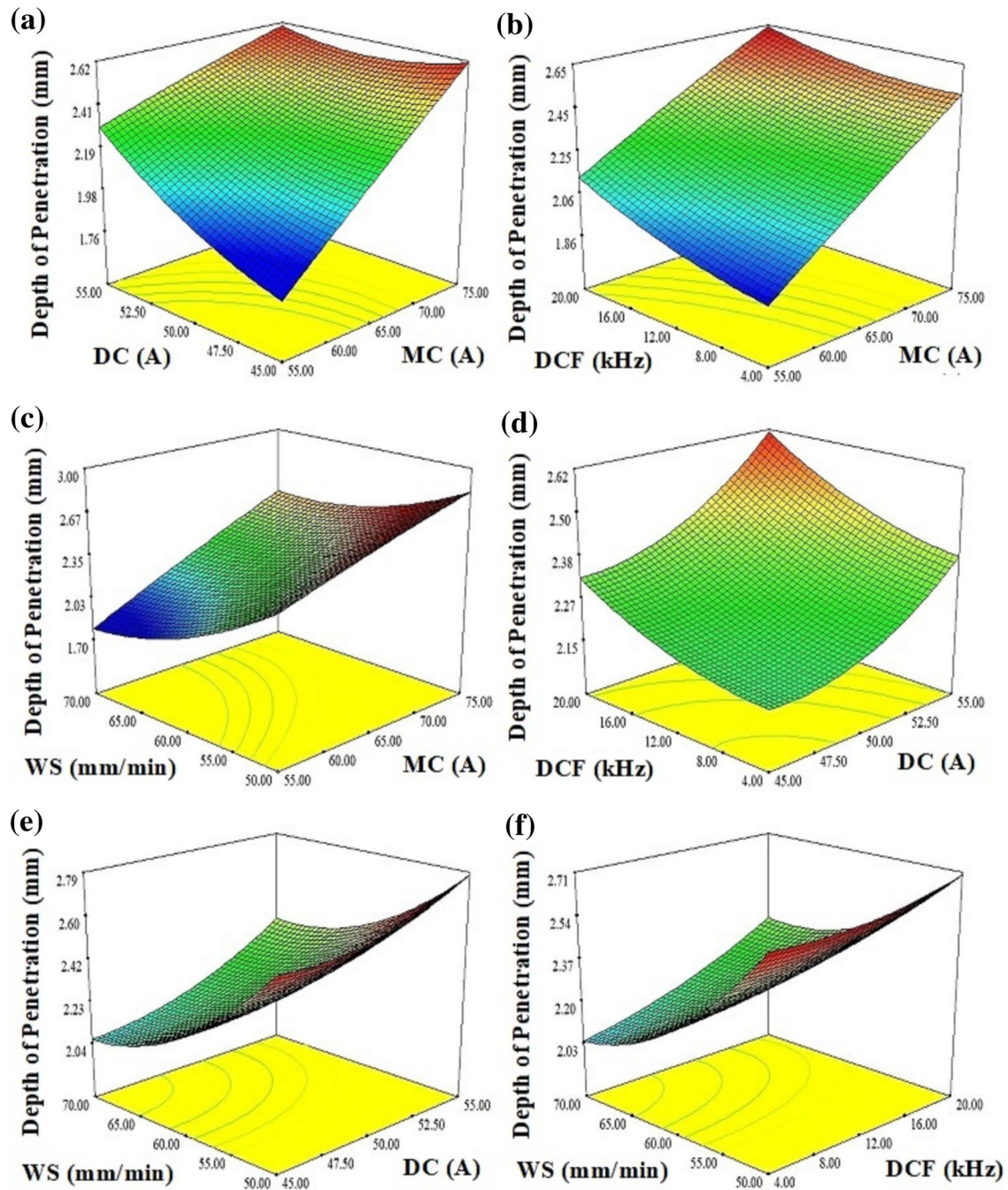


Fig. 14 3D Response Surface graphs for depth of penetration

A, DC of 47.5 A, DCF of 8 kHz and WS of 65 mm/min. Figure 16a shows the response surface plot for MC and DC assuming the DCF of 12 kHz and WS of 60 mm/min. It shows an interaction effect between MC and DC. It shows that increase in MC and DC leads to the rise in width of HAZ. The increase in width of HAZ is more significant above MC of 65 A and DC of 50 A. Figure 16b shows the response surface graph for MC and DCF assuming the DC of 50 A and WS of 60 mm/min. It shows an insignificant

interaction effect between MC and DCF. Figure 16c represents the response surface graph for MC and WS assuming the DC of 50 A and DCF of 12 kHz. It represents the interaction effect between MC and WS. It shows increase in width of HAZ at incremental levels of MC and WS. It is attributed to the fact that increase in MC is associated with increase in heat input. Also, an increase in WS at constant level of DC leads to the reduced arc constriction effect. This in turn provides wider arc and rise in width of HAZ.

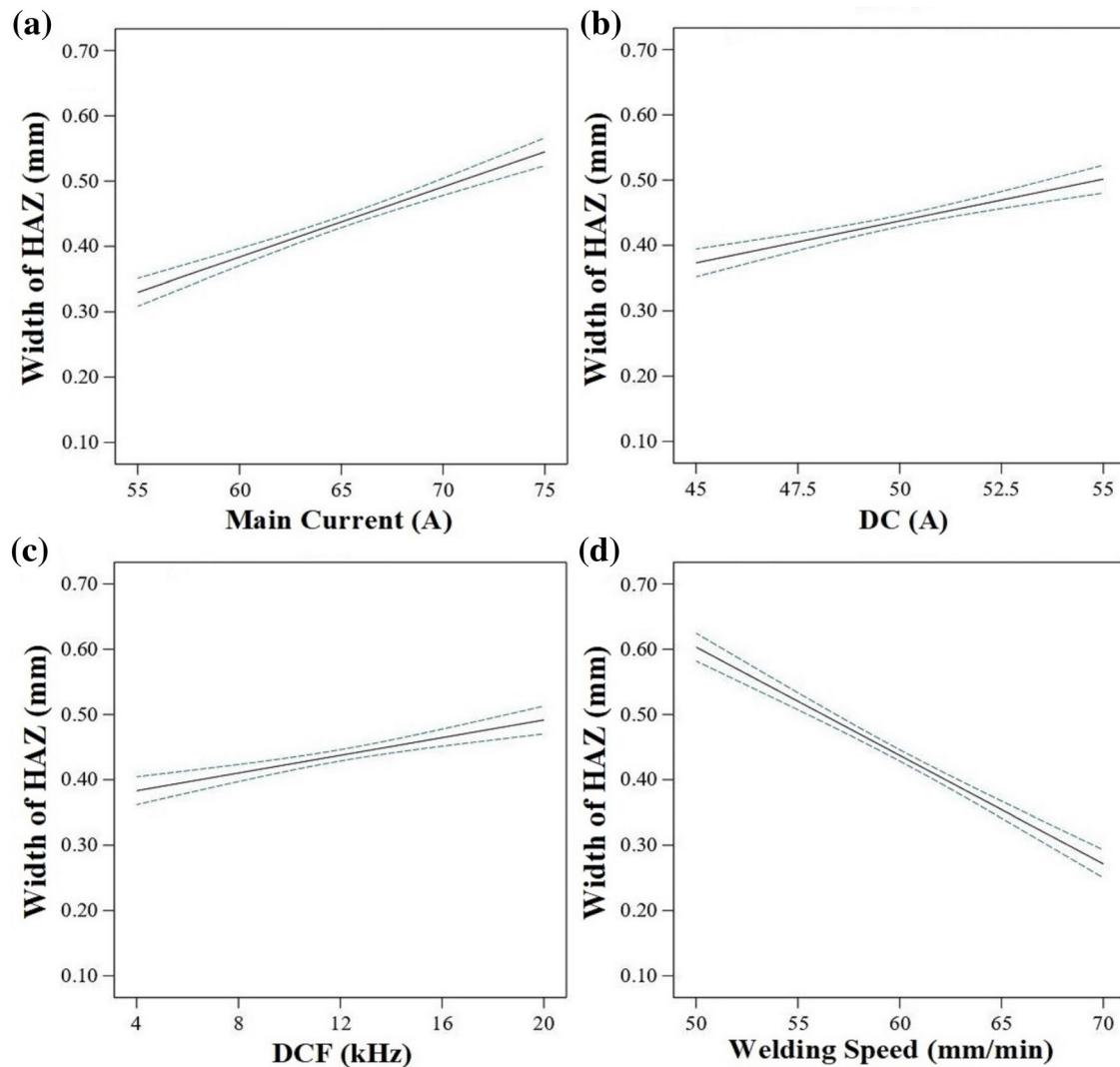


Fig. 15 Direct effect of GTCA welding parameters on width of HAZ

Figure 16d) represent the response surface graph for DC and DCF assuming the MC of 65 A and WS of 60 mm/min. It represents the insignificant interaction effect between DC and DCF. Figure 16e also shows that the interaction effect between DC and WS is insignificant. Figure 16f depicts the response surface graph for DCF and WS assuming the MC of 65 A and DC of 50 A. The interaction effect between DCF and WS is insignificant.

3.5.4 Direct and interaction effect of GTCA welding parameters on area of fusion zone

Figure 17a–d shows the direct effect of GTCAW parameters on the area of fusion zone. MC shows proportional curved linear relationship with the area of fusion zone. The area of fusion zone increases significantly above MC of 65 A. Increase in DC shows decrease in area of fusion zone up to

50 A. It is attributed to the increase in arc constriction which reduces the wastage of heat on outer flare and provides localized melting of metal at the joint. Further increase in DC results in increase in area of fusion zone. The increase in DC at constant level of WS leads to rise in heat input and more localized melting of metal at the joint. However, the direct effect of DC on area of fusion zone is less significant as compared to MC and WS. WS shows an inverse curved linear relationship with the area of fusion zone. MC and WS shows significant effect on area of fusion zone followed by DC and DCF.

Figure 18a–f represents the three-dimensional response surface graph for area of fusion zone. The optimum value of response is represented by the descent area of the response surface. It shows that the area of fusion zone is minimum at MC of 60 A, DC of 47.5 A, DCF of 8 kHz and WS of 65 mm/min. Figure 18a shows the interaction effect between

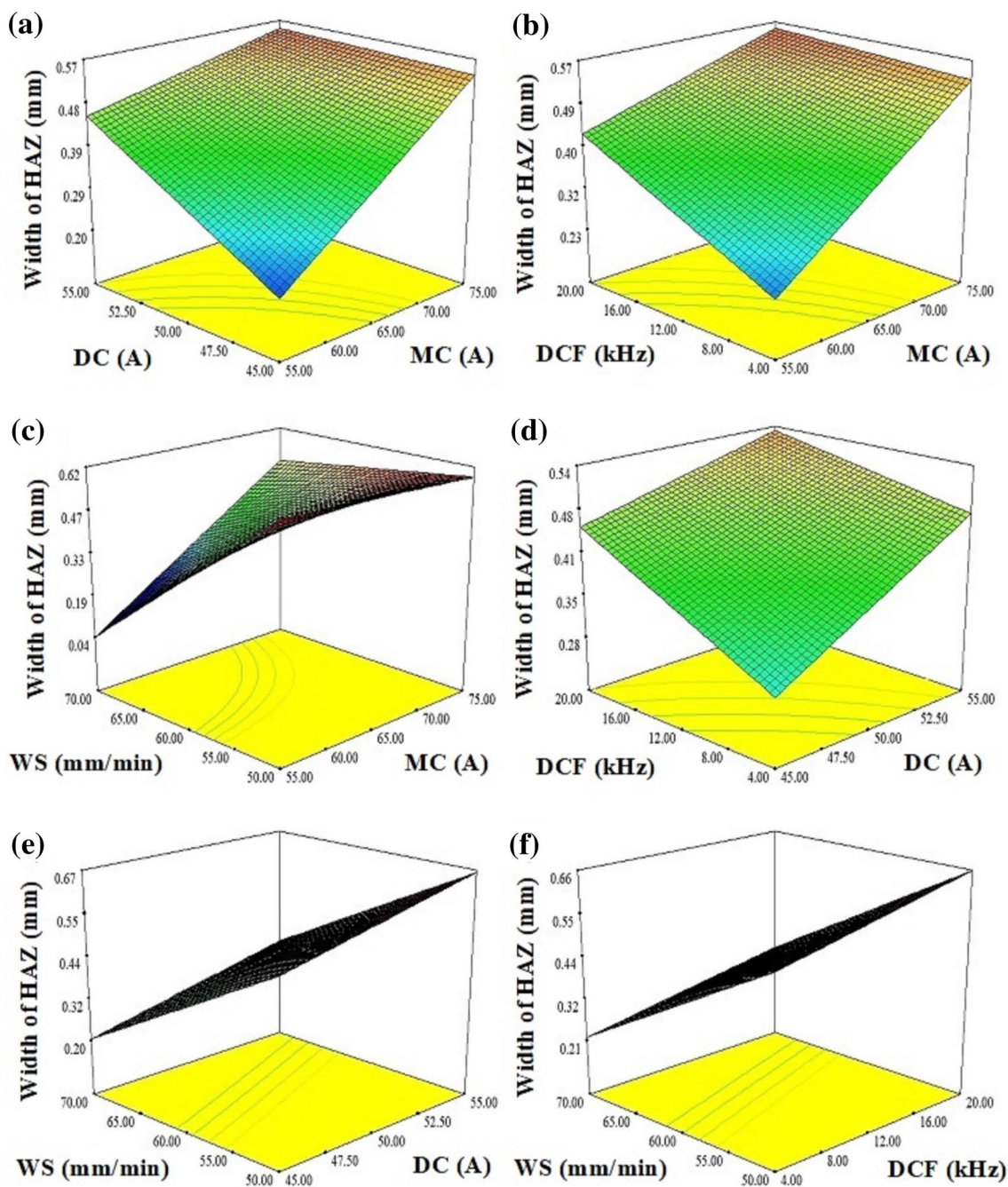


Fig. 16 3D Response Surface graphs for width of HAZ

MC and DC on the area of fusion zone assuming the DCF of 12 kHz and WS of 60 mm/min. It infers that increase in MC and DC results in an increase in area of fusion zone. This effect is more significant above MC of 65 A and DC of 50 A. It is attributed to the increase in heat input associated with incremental levels of MC and DC leading to the more melting of metal at the joint and rise in area of fusion zone. The area of fusion zone is observed to be larger at a higher level of MC (75 A) and DC (55 A). Figure 18b shows the

interaction effect between MC and DCF on the area of fusion zone assuming the DC of 50 A and WS of 60 mm/min. It indicates an increase in area of fusion zone at incremental levels of MC and DCF. It is attributed to the phenomenon of rise in heat input at incremental levels of MC and stacking of heat input in weld thermal cycle at increased levels of DCF. There is no significant effect up to MC of 65 A and DCF of 12 kHz. The rise in area of fusion zone at incremental levels of MC and DCF is more significant at higher level of 75 A

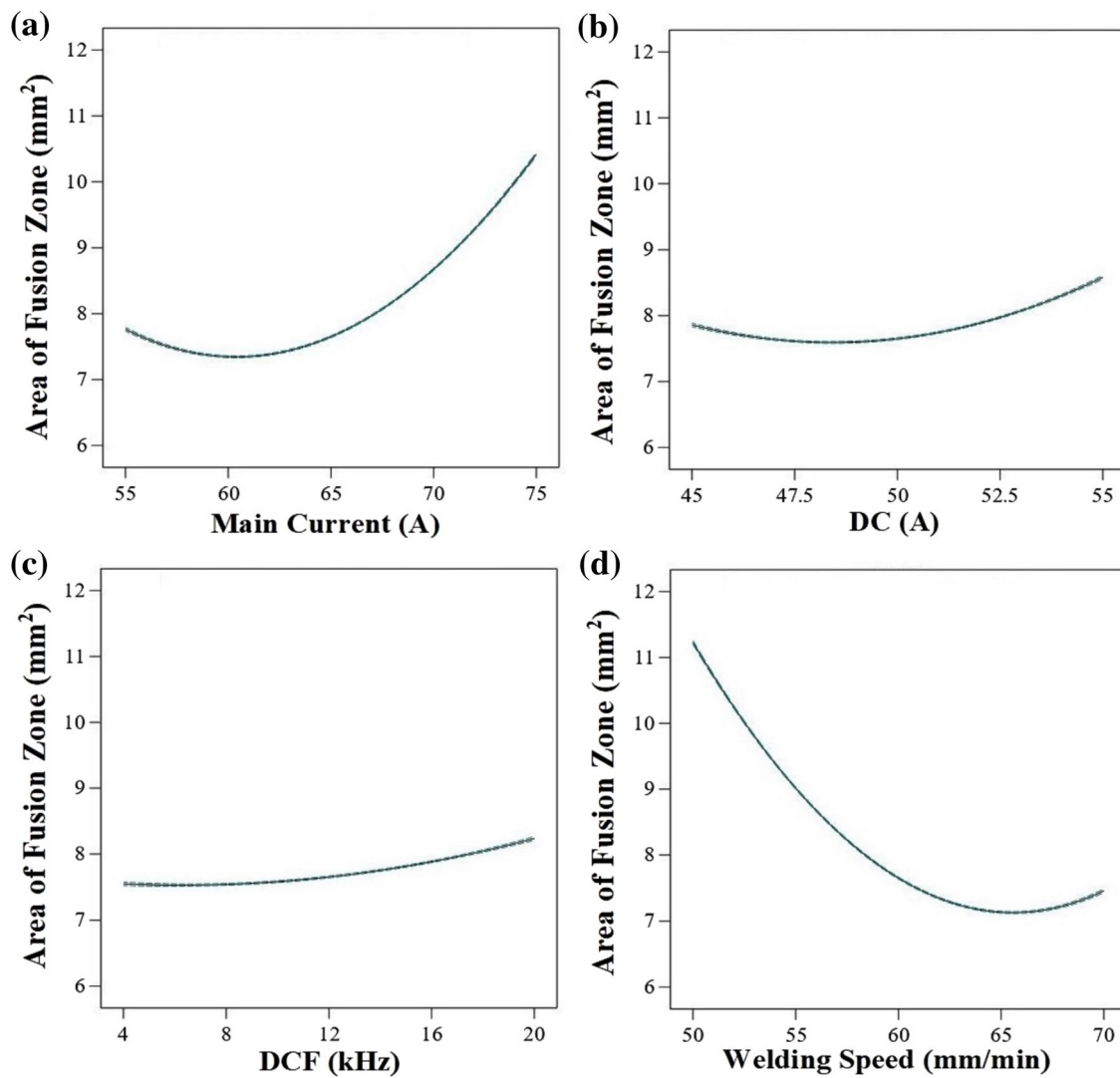


Fig. 17 Direct effect of GTCA welding parameters on area of fusion zone

and 20 kHz. Figure 18c shows the interaction effect between MC and WS on the area of fusion zone assuming the DC of 50 A and DCF of 12 kHz. It indicates that the area of fusion zone increases slightly at incremental levels of MC and WS. This effect is more pronounced at higher level of MC (above 65 A) and lower level of WS (below 50 mm/min).

Figure 18d shows interaction effect between DC and DCF on the area of fusion zone assuming the MC of 65 A and WS of 60 mm/min. It shows slight increase in the area of fusion zone at increased levels of DC and DCF. The interaction effect between DC and DCF is comparatively much less significant as compared to their respective direct effects on fusion zone. Figure 18e represents the interaction effect between DC and WS assuming the MC of 65 A and DCF of 12 kHz. It shows that increase in DC and WS shows

slight increase in area of fusion zone above DC of 52.5 A and WS of 65 mm/min. The interaction effect between DC and WS is more severe at all levels of DC and below WS of 60 mm/min. It shows larger weld bead area at DC of 45–55 A and WS of 50 mm/min. Increase in DC is associated with increase in arc constriction at incremental levels which provides localized melting of metal at the joint and minimizes the melting time. However, at lower WS there is more melting of metal at the joint and heat input effect is predominant. Figure 18f shows the insignificant interaction effect between DCF and WS assuming the MC of 65 A and DC of 50 A. Increase in DCF and WS shows slight increase in the area of fusion zone. However, it is observed to be larger at lower level of WS (50 mm/min) and higher level of DCF (20 kHz).

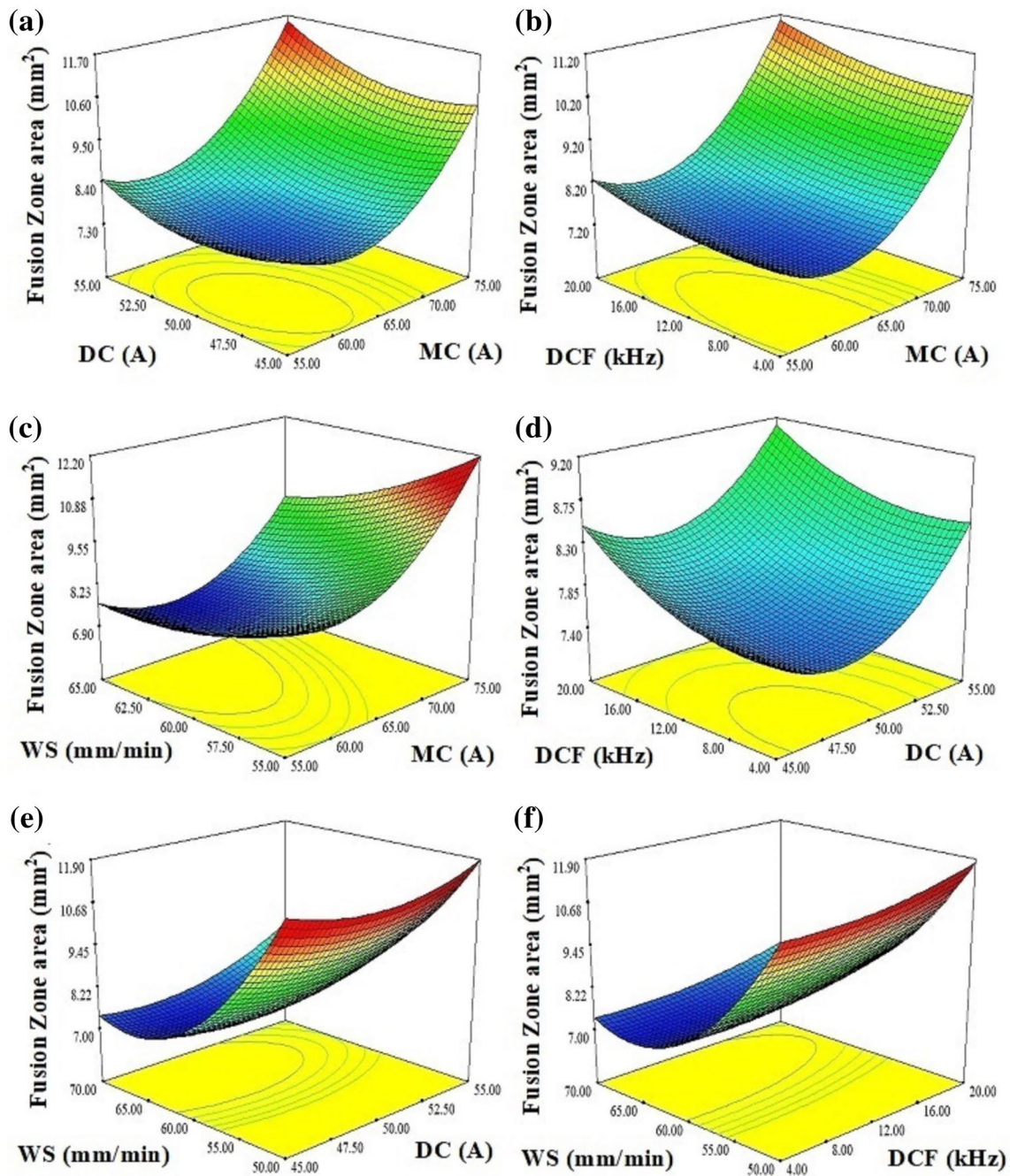


Fig. 18 3D Response Surface graphs for area of fusion zone

4 Conclusions

1. The GTCA welding parameters were optimized to attain full penetration with minimum weld bead geometry satisfying the optimality criteria. Thin Inconel 718 alloy sheets can be welded successfully using GTCAW process without porosity and hot cracking related defects.
2. The mathematical models were formulated to predict the weld bead characteristics (Width of Bead, Depth of

Penetration, Width of HAZ and Area of Fusion Zone) accurately with 95% confidence level. The optimal conditions and responses predicted by the RSM developed mathematical model showed proximity with the experimental optimum conditions and responses. It showed less than 4% error in predicting the weld bead characteristics.

3. Main Current and Welding Speed showed predominant influence on the weld bead characteristics, followed by Delta Current and Delta Current Frequency.
4. The 3D response surface graphs indicate that the beneficial effects of arc constriction and pulsing were not realized at higher levels of welding parameters. It is mainly attributed to the high heat input which extends predominant influence on the weld bead characteristics of joints compared to the magnetic arc constriction and pulsing.

Acknowledgements The authors express their deep sense of gratitude to the Director, Vikram Sarabhai Space Centre (VSSC), ISRO, Thiruvananthapuram, Kerala for providing base material to carry out this investigation and financial support through R & D project under RESPOND scheme (Project No. ISRO/RES/3/728/16–17).

Author contributions (optional: please review the submission guidelines from the journal whether statements are mandatory): Not Applicable.

Funding This project work is funded by Indian Space Research Organization (ISRO) India. Project No. ISRO/RES/3/728/16–17.

Data availability Not Applicable.

Compliance with ethical standards

Conflict of interest Not Applicable.

Code availability (software application or custom code): Not Applicable.

References

- Antony J (2003) Design of experiments for engineers and scientists. Heinemann, Oxford
- Balasubramanian M, Jayabalan V, Balasubramanian V (2008a) Developing mathematical models to predict tensile properties of pulsed current gas tungsten arc welded Ti-6Al-4V alloy. *Mater Des* 29:92–97. <https://doi.org/10.1016/j.matdes.2006.12.001>
- Balasubramanian M, Jayabalan V, Balasubramanian V (2008b) Developing mathematical models to predict grain size and hardness of argon tungsten pulsed current arc welded titanium alloy. *J Mater Proc Techno* 196:222–229. <https://doi.org/10.1016/j.jmatprotec.2007.05.039>
- Benyounis KY, Olabi AG, Hashmi MSJ (2005) Optimizing the laser-welded butt joints of medium carbon steel using RSM. *J Mater Proc Techno* 164:986–989. <https://doi.org/10.1016/j.jmatprotec.2005.02.067>
- Cao X, Rivaux B, Jahazi M, Cuddy J, Birur A (2009) Effect of pre- and post-weld heat treatment on metallurgical and tensile properties of Inconel 718 alloy butt joints welded using 4 kW Nd: YAG laser. *J Mater Sci* 44:4557–4571. <https://doi.org/10.1007/s10853-009-3691-5>
- Cortés R, Barragán ER, López VH, Ambriz RR, Jaramillo D (2017) Mechanical properties of Inconel 718 welds performed by gas tungsten arc welding. *Inter J Adv Manuf Technol* 94:3949–3961. <https://doi.org/10.1007/s00170-017-1128-x>
- Dong JX, Xie XS, Thompson RG (2000) The influence of sulfur on stress-rupture fracture in Inconel 718 superalloys. *Metall Mater Trans A* 31(9):2135–2144
- French R, Marin-Reyes H, Rendell-Read A (2017) A robotic remanufacturing system for high-value aerospace repair and overhaul. *Trans Intell Weld Manuf* 1:36–47. https://doi.org/10.1007/978-981-10-5355-9_3
- Henderson MB, Arrell D, Larsson R, Heobel M, Marchant G (2004) Nickel based superalloy welding practices for industrial gas turbine applications. *Sci Technol Weld Join* 9(1):13–21. <https://doi.org/10.1179/136217104225017099>
- Hong JK, Park JH, Park NK, Eom IS, Kim MB, Kang CY (2008) Microstructures and mechanical properties of Inconel 718 welds by CO₂ laser welding. *J Mater Proc Techno* 201:515–520. <https://doi.org/10.1016/j.jmatprotec.2007.11.224>
- Kiaee N, Aghaie-Khafri M (2014) Optimization of gas tungsten arc welding process by response surface methodology. *Mater Des* 54:25–31. <https://doi.org/10.1016/j.matdes.2013.08.032>
- Leary R, Merson E, Birmingham K, Harvey D, Brydson R (2010a) Microstructural and microtextural analysis of InterPulse GTCAW welds in Cp-Ti and Ti-6Al-4V. *Mater Sci Eng A* 527:7694–7705. <https://doi.org/10.1016/j.msea.2010.08.036>
- Leary R, Merson E, Brydson R (2010) Microtextures and grain boundary misorientation distributions in controlled heat input titanium alloy fusion welds. *J Phys: Conf Ser* 241:012103
- Liu Y, Zhang H, Guo Q, Zhou X, Ma Z, Huang Y, Li H (2018) Microstructure evolution of Inconel 718 superalloy during hot working and its recent development tendency. *Acta Metall Sin* 54:1653–1664. <https://doi.org/10.11900/0412.1961.2018.00340>
- Mei Y, Liu Y, Liu C, Li C, Yu L, Guo Q, Li H (2016) Effect of base metal and welding speed on fusion zone microstructure and HAZ hot-cracking of electron-beam welded Inconel 718. *Mater Des* 89:964–977. <https://doi.org/10.1016/j.matdes.2015.10.082>
- Montgomery DC (1997) Design and analysis of experiment. Wiley, New York
- Padmanaban G, Balasubramanian V (2011) Optimization of pulsed current gas tungsten arc welding process parameters to attain maximum tensile strength in AZ31B magnesium alloy. *Trans Nonferr Met Soc China* 21:467–476. [https://doi.org/10.1016/S1003-6326\(11\)60738-3](https://doi.org/10.1016/S1003-6326(11)60738-3)
- Pollock TM, Tin S (2006) Nickel-based superalloys for advanced turbine engines: chemistry. *Microstruct Properties J Prop Power* 22(2):361–374. <https://doi.org/10.2514/1.18239>
- Radhakrishna CH, Rao KP (1994) Studies on creep/stress rupture behaviour of superalloy 718 weldments used in gas turbine applications. *Mater High Temp* 12(4):323–327. <https://doi.org/10.1080/09603409.1994.11752536>
- Radhakrishna CH, Rao KP, Srinivas S (1995) Laves phase in superalloy 718 weld metals. *J Mater Sci Lett* 14:1810–1812. <https://doi.org/10.1007/BF00271015>
- Rajakumar S, Balasubramanian V (2012) Multi-response optimization of friction-stir-welded AA1100 aluminium alloy joints. *J Mater Eng Perform* 21:809–822. <https://doi.org/10.1007/s11665-011-9979-z>
- Ram GDJ, Reddy AV, Rao KP, Reddy GM (2005) Microstructure and mechanical properties of Inconel 718 electron beam welds. *Mater Sci Techno* 21:1132–1138. <https://doi.org/10.1179/174328405X62260>
- Ram GDJ, Venugopal Reddy A, Prasad Rao K, Madhusudhan Reddy G (2004) Control of Laves phase in Inconel 718 GTA welds with current pulsing. *Sci Technol Weld Join* 9:390–398. <https://doi.org/10.1179/136217104225021788>
- Ram GDJ, Venugopal Reddy A, Prasad Rao K, Reddy GM, Sarin Sundar JK (2005) Microstructure and tensile properties of Inconel

- 718 pulsed Nd-YAG laser welds. *J Mater Proc Techno* 167:73–82. <https://doi.org/10.1016/j.jmatprotec.2004.09.081>
- Razal Rose A, Manisekar K, Balasubramanian V, Rajakumar S (2012) Prediction and optimization of pulsed current tungsten inert gas welding parameters to attain maximum tensile strength in AZ61A magnesium alloy. *Mater Des* 37:334–348. <https://doi.org/10.1016/j.matdes.2012.01.007>
- Reddy GM, Srinivasa Murthy CV, Srinivasa Rao K, Prasad Rao K (2008) Improvement of mechanical properties of Inconel 718 electron beam welds—influence of welding techniques and post weld heat treatment. *Inter J Adv Manuf Techno* 43:671–680. <https://doi.org/10.1007/s00170-008-1751-7>
- Rodríguez NK, Barragán ER, Lijanová IV, Cortés R, Ambríz RR, Méndez C, Jaramillo D (2017) Heat Input Effect on the Mechanical Properties of Inconel 718 Gas Tungsten Arc Welds. *Proceed 17th Inter Conf New Trends in Fat and Fract* 255–262. https://doi.org/10.1007/978-3-319-70365-7_29
- Sivaprasad K, Ganesh Sundara Raman S, Mastanaiah P, Madhusudhan Reddy G (2006) Influence of magnetic arc oscillation and current pulsing on microstructure and high temperature tensile strength of alloy 718 TIG weldments. *Mater Sci Eng A* 428:327–331. <https://doi.org/10.1016/j.msea.2006.05.046>
- Sonar T, Balasubramanian V, Malarvizhi S, Venkateswaran T, Sivakumar D (2019) Effect of delta current and delta current frequency on tensile properties and microstructure of gas tungsten constricted arc (GTCA) welded Inconel 718 sheets. *J Mech Behav Mater* 28:186–200. <https://doi.org/10.1515/jmbm-2019-0020>
- Sonar T, Balasubramanian V, Malarvizhi S, Venkateswaran T, Sivakumar D (2020) Effect of heat input on microstructural evolution and tensile properties of gas tungsten constricted arc (GTCA) welded Inconel 718 sheets. *Metall Micro Anal* 9:369–392. <https://doi.org/10.1007/s13632-020-00654-1>
- Sudarshan Rao G, Saravanan K, Harikrishnan G, Sharma VMJ, Ramesh Narayan P, Sreekumar K, Sinha P (2012) Local deformation behaviour of Inconel 718 TIG weldments at room temperature and 550 °C. *Mater Sci Forum* 710:439–444. <https://doi.org/10.4028/www.scientific.net/MSF.710.439>
- Xie X.S, Dong JX, Zhang MC (2007) Research and Development of Inconel 718 Type Superalloy. *Mater Sci Forum* 539:262–269. <https://doi.org/10.4028/www.scientific.net/MSF.539-543.262>
- Zhang YN, Cao X, Wanjara P (2013) Microstructure and hardness of fiber laser deposited Inconel 718 using filler wire. *Inter J Adv Manuf Techno* 69:2569–2581. <https://doi.org/10.1007/s00170-013-5171-y>

Publisher's Note Springer Nature remains neutral with regard to jurisdictional claims in published maps and institutional affiliations.